Journal of Geochemical Exploration 196 (2019) 131–155

Contents lists available at ScienceDirect

Journal of Geochemical Exploration

journal homepage: www.elsevier.com/locate/gexplo

Petrology and geochemistry of scandium in New Caledonian Ni-Co laterites

Y. Teitler[a,*], M. Cathelineau[a], M. Ulrich[b], J.P. Ambrosi[c], M. Munoz[d], B. Sevin[e]

[a] Laboratoire GéoRessources, rue Jacques Callot, BP 70239, 54506 Vandoeuvre-lès-Nancy Cedex, France
[b] EOST, 1 rue Blessig, 67084 Strasbourg Cedex, France
[c] CEREGE, Aix-Marseille Université, CNRS, IRD, CdF, CEREGE, BP 80, 13545 Aix en Provence, France
[d] Geosciences Montpellier, CNRS UMR5243, Université de Montpellier, Place E. Bataillon, 34095 Montpellier, France
[e] Service de la Géologie de Nouvelle-Calédonie, Direction de l'industrie, des Mines et de l'Énergie, 1ter rue Unger, BP M2, 98849 Nouméa Cedex, New Caledonia

ARTICLE INFO

Keywords:
Scandium
Laterite
Ni-laterite
Goethite
New Caledonia

ABSTRACT

The growing demand for scandium (Sc), essential for several modern industrial applications, drives the mining industry to develop alternative Sc sources. In such context, significant Sc concentrations (~100 ppm) were recently reported in several Ni-Co lateritic oxide ores developed after mafic-ultramafic rocks. This contribution examines the distribution of Sc in Ni-Co laterites from New Caledonia, the sixth largest Ni producer worldwide. Representative lateritic profiles were selected based on the protolith type and include dunite, harzburgite and lherzolite protoliths, wherein the Sc content, determined by the relative proportion of olivine and pyroxene, ranges from < 5 ppm in dunite to > 10 ppm in lherzolite. In Ni-Co laterites, dissolution and leaching of primary Mg-rich silicates leads to the residual enrichment of iron as ferric oxides/oxyhydroxides in the upper horizons. Downward remobilization and trapping of Ni and Co lead to their local enrichment to economic concentrations, with maximum grades reached in the saprock/saprolite and in the transition horizons, respectively. In contrast, maximum Sc enrichment occurs in the yellow limonite horizon, where Sc-bearing goethite contains about ten times the Sc content of the parent rock. Consequently, harzburgite- and lherzolite-derived yellow limonites yield maximum Sc concentrations up to 100 ppm, together with moderate Ni and Co concentrations. There, Sc is potentially a valuable by-product that could be successfully co-extracted along with Ni and Co through hydrometallurgical processing. In addition to peridotite-hosted laterites, hornblende-rich amphibolites yield elevated Sc up to 130 ppm. The saprolitization of amphibolites leads to the formation of a goethite-gibbsite-kaolinite mixture with Sc concentrations > 200 ppm. There, goethite is the main Sc carrier with up to 800 ppm Sc. Therefore, despite their relatively limited volumes, amphibolite-derived saprolites may also represent attractive targets for Sc in New Caledonia. It is proposed that three main factors control the distribution and intensity of Sc enrichment in laterites derived from mafic and ultramafic rocks: (i) the initial Sc content of the parent rock, (ii) the development of goethite-dominated, yellow limonite after long-lived tropical weathering, and (iii) the local remobilization of Sc from the uppermost horizons through dissolution/recrystallization of goethite and partial replacement of goethite by hematite, thus leading to downward Sc concentration in the yellow limonite.

1. Introduction

Scandium (Sc), the 21st element of the periodic table, has several remarkable applications for the modern industry. The addition of small (< 1 wt%) amounts of Sc to Al dramatically increases its weldability and its resistance to stress, corrosion and heat, while maintaining a light weight (Royset and Ryum, 2005; Toropova et al., 1998). Scandium is therefore mainly used as hardening additive to aluminium to form Al-Sc alloys, with current applications in aerospace industries and manufacturing of high-quality sports equipment. In addition, Sc finds promising application in the development of Solid Oxide Fuel Cells (SOFCs), wherein the replacement of Y by Sc improves conductivity and lowers the operating temperature, extending fuel cell life. Also, Sc is notably used in high temperature lights, lasers and ceramics manufacturing.

Owing to its ionic radius and chemical properties, Sc has historically been regarded as a heavy rare earth element. Sc, which exclusively occurs in the +3 oxidation state, lacks affinity to combine with the common ore-forming anions. Thus, Sc^{3+} is typically not concentrated through geological processes and rarely forms Sc-rich minerals (Das et al., 1971; Emsley, 2014). Rather, it occurs as a trace element in a number of hydroxide, silicate, fluoride, sulfate and phosphate minerals.

* Corresponding author.
E-mail address: yoram.teitler@univ-lorraine.fr (Y. Teitler).

https://doi.org/10.1016/j.gexplo.2018.10.009
Received 13 April 2018; Received in revised form 2 October 2018; Accepted 16 October 2018
Available online 18 October 2018
0375-6742/

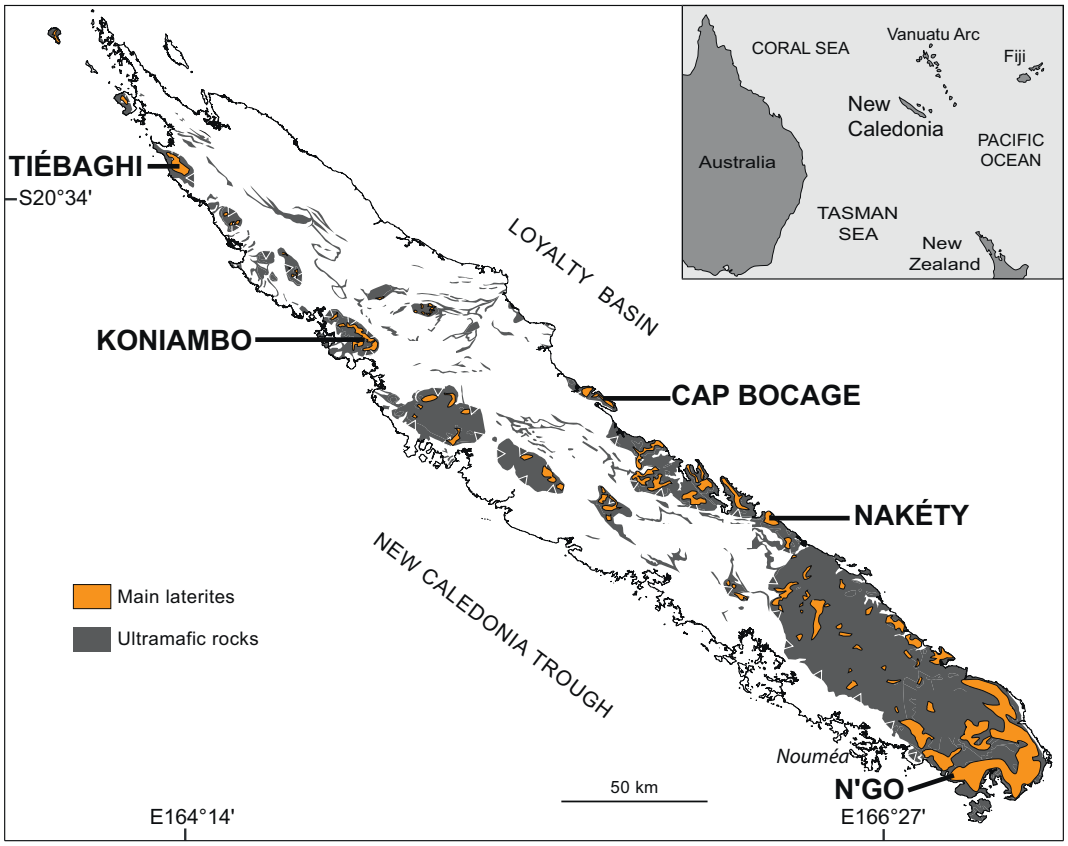

Fig. 1. Geological map of New Caledonia. Modified from Maurizot and Vendé-Leclerc (2009).

Consequently, although Sc is relatively common at the Earth's surface with an average crustal abundance of 22 ppm (Rudnick and Gao, 2014), it is only marginally produced (~15 t/yr, US Geological Survey, 2018) and solely as a by-product of uranium, tungsten, REE or titanium ore processing, most exclusively in China and to a lesser extent in Kazakhstan, Russia and Ukraine. So far, the quoted high prices and lack of an organized market for Sc have prevented its widespread commercial adoption. However, increasing needs in energy saving technologies together with recent development of Sc extraction techniques have raised interest for this metal. In the last decade, Sc-rich occurrences with economically attractive grades and tonnages have been identified in some oxide-rich laterites developed after mafic and ultramafic rocks (Aiglsperger et al., 2016; Audet, 2008; Bailly et al., 2014; Chassé et al., 2017; Hoatson et al., 2011; Maulana et al., 2016; Ulrich et al., submitted). There, Sc enrichment is interpreted to be largely residual, resulting from the intense leaching of mobile cations during lateritization of the parent rock, while Sc remains trapped and concentrated in neoformed goethite. The initial Sc content of the parent rock is, therefore, of primary importance in controlling the Sc concentrations in its weathered derivatives. Two main types of Sc-bearing laterites are distinguished, depending on the parent rock type. First, oxide-rich laterites developed after clinopyroxenites may yield Sc concentrations typically ranging from 300 to 600 ppm and locally up to 800 ppm (Chassé et al., 2017). To date, two high-grade (> 300 ppm) Sc lateritic districts, both located in New South Wales, Australia, have been identified and are under development for exploitation: the Syerston-Flemington-Owendale and the Nyngan districts. These laterites, considered as worldclass Sc deposits, are developed from Alaskan-type clinopyroxenites which yield unusually high Sc concentrations of about ~80 ppm (Chassé et al., 2017). The lateritization of these Sc-rich clinopyroxenites resulted in a fourfold to tenfold increase of the Sc concentration, explaining the atypically elevated Sc grades (300–600 ppm and up to 800 ppm) identified in their lateritic derivatives. Second, oxide-rich Ni-Co laterites developed after peridotites may yield Sc content up to 60–100 ppm, as observed in some Ni-Co laterites from Queensland (Australia), New Caledonia, Philippines and the Cuba - Hispaniola islands of the Greater Antilles (Aiglsperger et al., 2016; Audet, 2008; Maulana et al., 2016; Hoatson et al., 2011). Previous investigations (Aiglsperger et al., 2016; Maulana et al., 2016; Audet, 2008; Ulrich et al., submitted) showed that maximum Sc grades are observed in the goethite-dominated, yellow limonite horizon, representing about a tenfold enrichment compared to the parent peridotite, with higher Sc grades (100 ppm) being reached in harzburgite-derived laterites compared to dunite-derived laterites (60 ppm). Such concentrations are too low to be economically attractive as standalone Sc resources. Nevertheless, Sc could be a highly valuable by-product of Ni and Co processing, provided that (i) Sc-rich zones sufficiently overlap Ni- and/or Co-rich zones, and (ii) metallurgical plants allow extraction of Sc along with Ni-Co ore processing. Recently, several mining companies have developed industrialized plants for Sc recovery from Ni-Co laterites, demonstrating successful and cost-effective recovery of Sc from the hydrometallurgical extraction of lateritic Ni-Co ores (Ricketts and Duyvesteyn, 2018). Among the primary producers of lateritic nickel and cobalt that may develop Sc co-beneficiation, opportunities exist for New Caledonia, as (i) its Ni (+Co) resources, accounting for about 11% of the world nickel resources, are dominantly hosted in oxide laterites, which are considered as the most favorable ore type for Sc co-valorization, and (ii) the hydrometallurgical processing plant currently operated by Vale in the Goro mine (South Province) could allow operators to extract Sc directly on site using ion exchange and solvent extraction techniques (Altinsel et al., 2018; Ferizoglu et al., 2018; Wang et al., 2011). Additionally, some occurrences of weathered, amphibole-rich intrusive rocks have been recognized across the New Caledonian peridotite nappe (Cluzel et al., 2006). Such lithologies may host elevated amounts of Sc, close to that of the high-grade (300 ppm or higher), clinopyroxenite-derived laterites from the Syerston-Flemington

and Nyngan deposits in Australia. In this contribution we examine the distribution of Sc in representative lateritic sequences of New Caledonia, accounting for the different types of protoliths and alteration styles. These include currently mined Ni-Co laterites developed after peridotites, wherein Sc may be a valuable by-product of Ni-Co production, as well as laterites developed after amphibole-rich, mafic intrusive bodies. Using a combination of field characterization, petrology, whole-rock and in situ major and trace element geochemistry, we address the major processes and the critical controls on Sc enrichment and discuss the economic potential for Sc recovery in New Caledonian laterites.

2. Regional geology

The New Caledonian archipelago, comprising several islands distributed along the Norfolk and Loyalty ridges in the South West Pacific, constitutes the emerged northern tip of the Zealandia continent, formerly part of the Gondwana supercontinent (Mortimer et al., 2017). The main island, referred to as "Grande Terre" (Fig. 1), consists of a 300 km long allochtonous peridotite ophiolite tectonically overlying continental rock sequences of the Norfolk Ridge (Cluzel et al., 2012a). The geological evolution of New Caledonia includes several tectonic phases. Importantly, the North-east-dipping subduction, which appeared to the East of New Caledonia at the Paleocene-Eocene boundary, ended during the Late Eocene with the obduction of the peridotite ophiolite after blocking of the subduction zone by the Norfolk Ridge at ca. 35 Ma (Cluzel et al., 2001, 2012a; Paquette and Cluzel, 2007). The Peridotite Nappe, which hosts the Ni-Co lateritic resources of New Caledonia, represents about 30% of the surface of Grande Terre. Exposed in the "Massif du Sud" and in several isolated tectonic klippes, mainly aligned in the N140 direction along the west coast of the island (Koniambo, Tiebaghi, Poum massifs), the Peridotite Nappe is mostly composed of harzburgite locally interlayered with dunite, except in the northernmost klippes where lherzolite dominates (Ulrich et al., 2010). In the Massif du Sud, peridotites are locally overlain by wehrlites and layered cumulate gabbros, representing remnant of the subduction-related magmatic crust (Marchesi et al., 2009; Prinzhofer, 1981). The nappe does not exhibit any major internal thrusts and, therefore, did not experience thickening during its tectonic emplacement. Slab dehydration during Eocene subduction lead to forearc mantle serpentinization (Frost et al., 2013; Ulrich et al., 2016). In the main part of the nappe, serpentines principally occur as networks of mm- to ~10 cm-thick fractures and veins containing lizardite ± chrysotile. In contrast, the base of the peridotite nappe consists of a 20 to 200 m thick, subhorizontal, porphyroclastic and mylonitic serpentinite sole formed during obduction, containing up to 100% serpentine (Avias, 1967; Orloff, 1968; Guillon, 1975; Cluzel et al., 2012a; Quesnel et al., 2013; Ulrich et al., 2016). Locally, amphibolite lenses occur at the base of the serpentine sole, above the Poya Basalt formation. These lenses are regarded as tectonic slices of the South Loyalty basin oceanic crust that recrystallized at ca. 56 Ma into the high-temperature amphibolite facies (Cluzel et al., 2012b). Also, ultramafic-mafic (amphibolite to microdiorite), and felsic (leucodiorite to granite) coarse grain dykes are developed throughout the Peridotite Nappe, especially in the Massif du Sud. These dykes, dated at ca. 53 Ma, are interpreted as slab melts and supra-subduction zone magmatic products (Cluzel et al., 2006). Subsequently, the emersion of New Caledonia during or soon after obduction lead to the development of a thick regolith cover that likely extended over the whole island. Several stepped planation surfaces were developed during repeated uplift phases and/or seas level changes until the Oligocene (Chardon and Chevillotte, 2006). In the northern part of the Grande Terre, the laterite-blanketed peridotite has since been intensively eroded and dissected, so that it only remains as isolated klippes along the west coast of the island, whereas it is largely preserved in the southern lowlands and endorheic basins of the South Massif, where weathering probably continued until recently (Sevin et al., 2012, 2014). Some occurrences of pseudo-karstic structures in the peridotite nappe demonstrate the existence of an efficient drainage system (Genna et al., 2005; Jeanpert et al., 2016; Trescases, 1975). Importantly, the extensive lateritization of the peridotite ophiolite resulted in the formation of the worldclass lateritic Ni-Co resources mined in New Caledonia. Genetic models for Ni-Co laterites in New Caledonia involve (i) the leaching of most elements including Mg and Si after hydrolysis of olivine (0.4% Ni) and pyroxene (0.025% Ni), (ii) the redistribution and concentration of Ni within the saprock as secondary hydrous silicates, locally grading over 20% Ni (related to garnierite veins), (iii) the development of Ni-bearing saprolite, containing both silicates and oxides, at the expense of the saprock, and (iv) the development of oxide-rich, Ni-bearing limonite and ferricrete at the expense of the saprolite (Butt and Cluzel, 2013; Cathelineau et al., 2016, 2017; Freyssinet et al., 2005; Golightly, 2010; Manceau et al., 2000; Trescases, 1975; Wells et al., 2009). The Ni-rich, silicate ± garnieritic ore has been actively mined since the late 19th century but reserves are rapidly being depleted. The overlying lateritic ore ("limonite") yields lower Ni concentrations (1.0–1.5% Ni). However, laterite ore reserves are enormous and will represent the bulk of Ni reserves of New Caledonia in the future. Also, Ni laterite ores often yield elevated (> 2000 ppm) cobalt concentrations adding significant value to the ore. Currently, co-extraction of Ni and Co from oxide laterite ore is successfully applied at the Goro processing plant (Massif du Sud). Similarly, Sc may add significant value to lateritic Ni(-Co) ore as it is assumed to be concentrated in the yellow limonite horizon. Although lateritic profiles in New Caledonia mostly consist of a saprolitic zone with mixed hydrous silicates and oxides that directly grades upwards into a limonitic zone essentially composed of oxides and oxyhydroxides, a few lateritic profiles exhibit well-developed, Ni-rich smectitic zones below the limonite. The development and preservation of Ni smectitic ore, mostly observed in Tiébaghi Ni-laterites and more locally in some low-altitude laterites of the Boulinda massif (Latham, 1986; Trescases, 1975), probably relates to relatively lower drainage conditions during weathering. As suggested by previous studies documenting the distribution of Sc in some dunite- and harzburgite-derived Ni laterites from New Caledonia, both the type of peridotite protolith and the styles of lateritic weathering are important parameters controlling the maximum Sc grades (Audet, 2008; Bailly et al., 2014). So far, no data is available on Sc in lherzolite-derived Ni-laterites, although Ulrich et al. (submitted) observed Sc contents up to 20 ppm in some unweathered lherzolites. Differences in the Sc content of peridotites likely relate to their variable proportions of magnesian olivine (forsterite), orthopyroxene (enstatite) and clinopyroxene (diopside). With regards to the mafic intrusive rocks documented by Cluzel et al. (2006), no data on Sc is available neither on the unweathered lithologies nor in their lateritic derivatives. In the following, we document and discuss the distribution of Sc in some representative mafic- and ultramafic-derived lateritic profiles of New Caledonia.

3. Methodology

3.1. Sampling strategy

In order to investigate the Sc distribution in representative laterites from New Caledonia, a sampling strategy was developed to encompass the diversity of peridotitic (harzburgite, dunite, lherzolite ± serpentinite) and mafic to ultramafic intrusive (gabbro, pyroxenite, amphibolite) protholiths. Selected Ni-laterites include (i) six harzburgite-derived laterites from Koniambo massif, N'Go (Massif du Sud), Nakéty (Nakéty-Dothio massif) and Cap Bocage (Monéo massif), (ii) two dunite-derived laterites from Cap Bocage and N'Go, and (iii) two lherzolite-derived, atypical smectite-rich laterites from Tiébaghi (Fig. 1). Selected lateritic profiles are mostly preserved from erosion and were sampled from the bedrock to the ferricrete. Sampling was mainly conducted on 15 to > 60 m deep diamond drill holes that

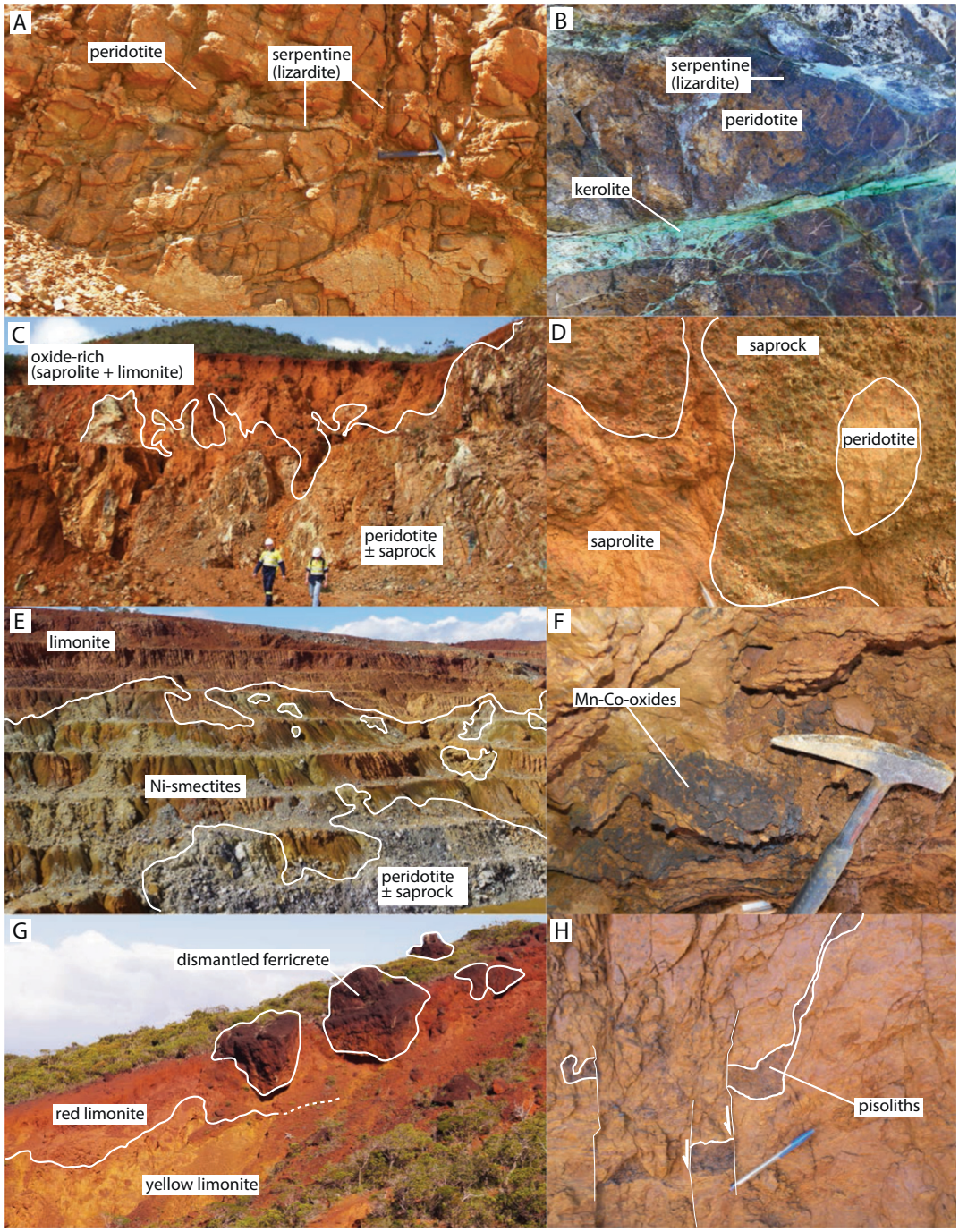

Fig. 2. Field photographs of peridotite-derived laterites. (A) Unweathered harzburgite with networks of serpentine (lizardite) veins (Koniambo), (B) Ni-rich talc-like (kerolite) vein developed at the bedrock – saprock interface (Koniambo), (C) Typical sharp transition from silicate-dominated bedrock and saprock to oxide-dominated saprolite and limonite (Koniambo). (D) Altered boulder of peridotite grading outwards from unweathered dunite to saprock and saprolite. The saprock is poorly developed (< 20 cm in thickness) and readily grades into oxide-dominated saprolite (Cap Bocage). (E) Well-developed Ni smectite-rich zone (up to > 15 m in vertical thickness) above lherzolitic serpentinite at Tiébaghi. (F) Mn-Co oxide-rich transition zone developed at the saprolite – yellow limonite interface (Cap Bocage). (G) Yellow limonite grading upwards into red limonite. The red limonite encapsulates boulders of the dismantled ferricrete (Tiébaghi). (H) Neptunian dyke of pisolithic material into the yellow limonite (Cap Bocage).

penetrated the near-surface weathering down to the bedrock. Drill cores were logged in terms of their rock types, serpentinization intensity and weathering intensity. Drill hole sampling was twinned with field observations in corresponding open pits when accessible. Complementary sample collection was conducted along open pit walls for some key facies and profiles when accessible and necessary (i.e. no drill cores available). Also, five amphibolite or amphibole-bearing pyroxenite dykes and their lateritic derivatives were sampled in N'Go and Nakéty, together with two profiles of lateritized gabbro dykes and their peridotite-derived laterite hosts in Koniambo and N'Go. In addition, discrete samples of pristine amphibole-bearing gabbros were collected in N'Go, Nakéty and Tiébaghi. Laterites developed after wehrlites or gabbro cumulates, locally exposed in the Massif du Sud, were not investigated in the present study. Location coordinates are given using the RGNC Lambert NC geographic coordinate system.

3.2. Analytical strategy

Sixty polished thin-sections were prepared from collected samples and examined using reflected/transmitted light and scanning electron microscopy with a JEOL JSM7600F at Georessources Laboratory and at SCMEM. In situ mineral chemistry analysis for major elements (Na, Mg, Al, Si, P, Ca, Ti, Mn, Fe, Co, Ni) was conducted using a CAMECA SX100 electron microprobe (EPMA, WDS analysis) at the SCMEM with typical beam conditions of 15 kV and 10 nA. In situ analysis for Sc and other trace elements was conducted using either an electron microprobe or LA-ICP-MS (193 nm MicroLas ArF Excimer coupled with Agilent 7500c quadrupole ICP-MS). Specific beam conditions for the electron microprobe WDS analysis of Sc were 25 kV and 150 nA, with both the detection limit and accuracy of about 50 ppm. LA-ICP-MS analysis of Sc in silicates was performed with the NIST60 standard. For oxides, in-house standards were developed and validated (Ulrich et al., submitted). Detection limit was below 2 ppm for most trace elements. Ablation time and spot sizes were 45 s and 60 µm, respectively. Data processing was conducted using the SILLS program (Guillong et al., 2008).

Hand specimens were crushed using an agate bowl pulveriser at GeoRessources Laboratory, and pulps were analyzed for whole-rock major- and trace-element geochemistry at the SARM analytical service of the CRPG using the procedure of Carignan et al. (2001). Major element oxides and Sc were analyzed using an iCap6500 ICP-OES with Li borate fusion. Trace elements were analyzed using an iCapQ ICP-MS with Li borate fusion followed by nitric acid digestion. The loss on ignition (LOI) component was determined by drying sample powders overnight at 110 °C, ignition at 1100 °C and subsequent measurement of the weight loss. Analytical accuracy (2 s standard deviation) lies within typical uncertainty of the analytical data for both major oxides and trace elements, that is < 1% for major oxides and < 5% for most trace elements.

4. Geology of investigated sites

4.1. Ni-Co laterites developed after peridotites

In the five investigated districts (Fig. 1), Ni-Co laterites exhibit a suite of alteration facies with specific mineral assemblages and composition. All the Ni-Co laterites are developed after serpentinized peridotites of variable type. At Koniambo and Nakéty, harzburgite is predominant. At N'Go and Cap Bocage, harzburgite also dominates but it is interlayered with significant volumes of dunite. At Tiébaghi, lherzolite dominates over harzburgite, although the intensive serpentinization of the peridotite complicates its univocal recognition in the field. The intensity of serpentinization in unweathered peridotites is variable and relates, at the district- to regional-scale, to the vertical proximity of the peridotite with the serpentine sole developed at the base of the ophiolite nappe (positioned at ca. 200 m in elevation). Tiébaghi Ni-Co laterites, located at low altitude (200–400 m), are therefore developed from intensely serpentinized peridotites. In contrast, in Ni-Co laterites developed at higher altitude (e.g. Koniambo massif laterites positioned at 900 m, i.e. well above the serpentine sole), serpentinization mostly occurs as mm to dm-large veins of serpentine distributed as fracture networks within the peridotite (Fig. 2A).

Saprolitization of the peridotite initiates along fractures, often using pre-existing structures, and progresses pervasively from these fractures into the fresh peridotite boulders. There, hydrolysis of olivine and pyroxene results in an increase in porosity while largely maintaining hardness. Diffuse greenish coloration of the saprock likely relates to an increase of the Ni content (Fig. 2D). Ni-rich (up to 15–20 wt% Ni), greenish talc-like (kerolite) veins are best expressed in the saprock and root into the fresh peridotite (Fig. 2B). The saprock is usually poorly developed in thickness (< 50 cm) and sharply evolves upwards into the saprolite (e.g. in the OPB7 profile, Koniambo, Fig. 3A) wherein

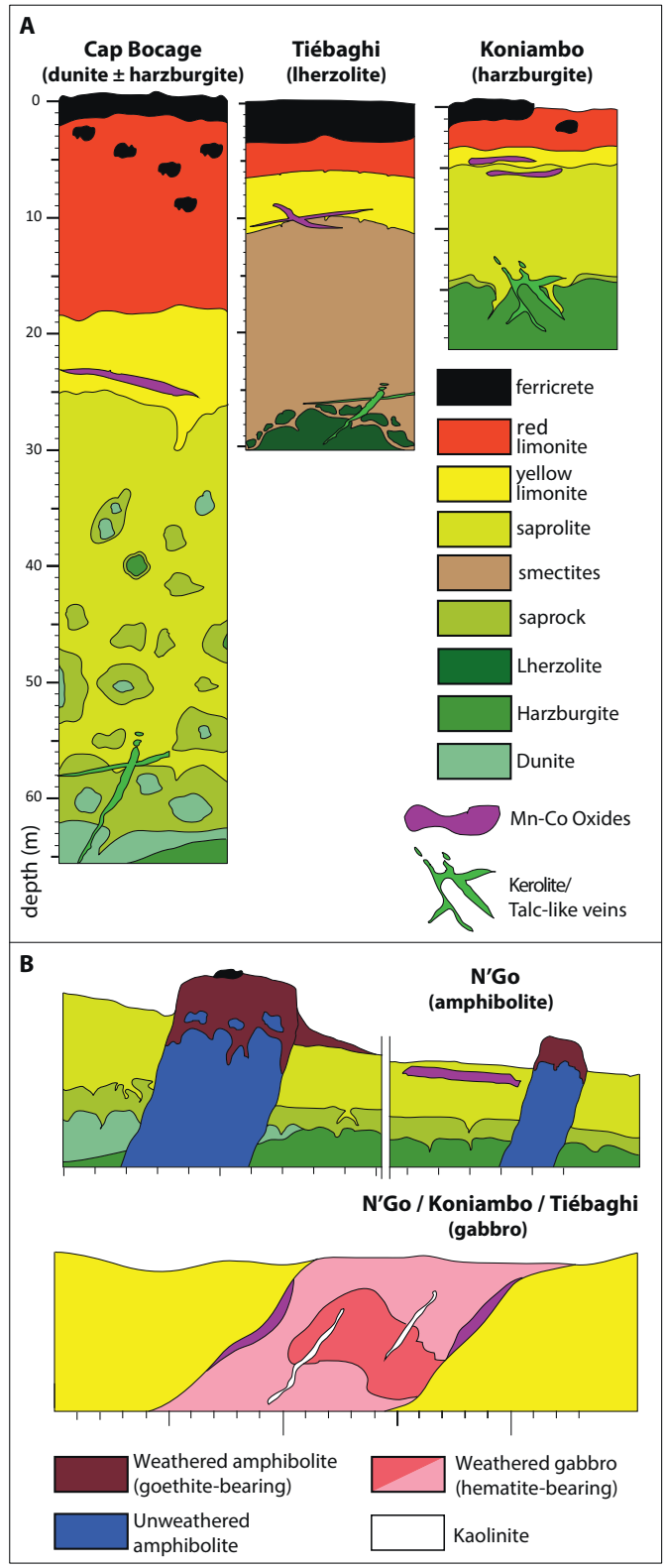

Fig. 3. Stratigraphic logs and cross sections of representative laterites (A) Peridotite-derived laterites. (B) Amphibolite- and gabbro-derived laterites.

weathering is more pronounced but remains isovolumetric (Figs. 2C, D, 3A). In some other profiles, the saprock may be thicker (~3 m) and remains partly preserved as hard cores within the overlying saprolite (e.g. in the PZ1B profile, cap Bocage, Fig. 3A). Although saprolitic material is friable, primary structures remain essentially preserved with

minimal compaction, further increasing the porosity so that the bulk density of dry saprolite may drop below 1 (referred to as "minerais bouchon" or "cork ore" by local miners for its buoyancy properties). It is worth noting that some atypical lateritic profiles exhibit well developed Ni smectite-rich zones below the oxide-rich zone (Figs. 2E, 3A). Such laterites are mostly developed in the northernmost klippes and particularly at Tiébaghi (Fantoche, East and South Alpha deposits). Also, similar extensive occurrences of Ni-smectites were recognized during our investigations in the Ma-oui deposit of the Koniambo mine.

The interface between the saprolite and the overlying limonite, referred to as the transition zone, is marked by the progressive disappearance of primary structures and the subsequent compaction of the saprolite. The transition zone often exhibits significant concentrations of Mn-Co-Ni oxides (lithiophorite, asbolane) either as mm- to cm-thick veins or as diffuse accumulations in the iron-rich matrix (Figs. 2F, 3A). The transition zone evolves upwards into the usually well-developed yellow limonite wherein ochreous goethite predominates. The yellow limonite then grades into the red limonite wherein hematite forms at the expense of ochreous goethite resulting in a mineral assemblage dominated by goethite but containing significant amounts (> 5 vol%) of hematite. Eventually, lateritic profiles are capped by massive to vesicular ferricrete and pisolithic horizons. These uppermost units are largely dissected and dismantled by erosion so that boulders of the ferruginous hardcaps often appear encapsulated in the underlying loose limonitic material (Figs. 2G, H, 3A).

4.2. Laterites developed after mafic-ultramafic intrusive rocks

The mafic dykes identified at N'Go, Nakéty and Tiébaghi display a suite of texture and mineralogy. Amphibolite and amphibole-bearing pyroxenite exposed in N'Go and Nakéty occur as subvertical dykes, locally forming swarms, with thickness ranging from < 10 cm up to > 10 m (Figs. 3B, 4A). Amphibolites and amphibole-bearing pyroxenites are commonly more resistant to weathering than the surrounding peridotites and, therefore, form positive relief in outcrops (Fig. 4A). These dykes contain variable proportions of amphibole and pyroxene, from amphibole-bearing pyroxenites where pyroxene dominates to amphibolites essentially composed of amphibole, and exhibit variable crystal sizes, from fine-grained (pyroxene and amphibole < 1 mm) to pegmatitic (amphibole up to 10 cm, pyroxene up to 5 mm) textures. Such variability is observed down to the outcrop scale, where two adjacent dykes often display marked differences in thickness, texture and/or composition. Noteworthily, one large (> 10 m thick) intrusive body identified at N'Go shows internal zonation of texture and mineralogy, from zones consisting of monomineralic amphibolite to zones dominated by pyroxene with giant (> 10 cm) amphibole porphyroblasts (Fig. 4E). Similarly, dykes of amphibole-bearing gabbros identified in Tiébaghi, N'Go, Nakéty (Fig. 4F) display variable crystal size, from fine grained to pegmatitic texture, and contain variable proportion of feldspar (~50 to 90 vol%) and amphibole (~10 to 50 vol%).

Due to their increased resistance to weathering, amphibolites and amphibole-bearing pyroxenites exposed in outcrops exhibit alteration that generally penetrates only to shallow depth (few cm to few m) below the surface, contrasting with the well-developed laterite profiles derived from peridotites (15 to 60 m in thickness). The most evolved weathering product of these dykes consists of brownish, goethite-bearing saprolitic material, wherein primary silicates have been largely leached away although primary structures remain preserved. *Stricto* sensu lateritic horizons, i.e. with obliterated textures, are rarely observed. Owing to the positive relief formed by these dykes relative to the surrounding peridotite-derived laterites, fragments of amphibolite- or pyroxenite-derived saprolite may accumulate downslope from outcrops (Fig. 4A). Comparatively, amphibole-bearing gabbros are more readily altered as they mainly contain weatherable feldspar, so that they may alter to greater depth and form friable lateritic material (Fig. 4B). Importantly, whereas amphibolite and pyroxenite usually alter to form brownish, goethite-bearing saprolite, gabbro alters to pinkish, hematite- and kaolinite-bearing saprolite/limonite (Fig. 4B). Color zonation patterns are commonly observed in weathered gabbros, from whitish or pale pinkish facies dominated by kaolinite, to cherry pinkish facies with higher proportions of hematite (Fig. 4D). Such zonation likely results either from primary zonation in the gabbro or secondary segregation of Fe and Al during weathering. As discussed below, the observed discrepancy in the nature of secondary iron-bearing phases (goethite vs. hematite) formed through weathering of mafic-ultramafic dykes (amphibolite and pyroxenite vs. gabbro) is of major importance in controlling Sc distribution in their weathered derivatives.

5. Scandium in parent rocks

5.1. Peridotites

5.1.1. Mineral assemblages

Unweathered peridotites exhibit typical mineral assemblages including (i) primary (mantle-derived) magnesian olivine (forsterite), orthopyroxene (enstatite) and clinopyroxene (diopside), whose relative proportions depend on the type of peridotite, and (ii) secondary (developed at the expense of mantle silicates) serpentine (mainly lizardite), whose relative proportion depend on the degree of serpentinization. In dunite, as observed at N'Go and Cap Bocage, forsterite is the predominant (> 90 vol%) mantle silicate (Fig. 5A–C) while enstatite may only be present as an accessory phase, both mineral forming automorph crystals up to ~8 mm. Accessory chromiferous spinel is also commonly observed (Fig. 5C). Comparatively, harzburgite exhibits a higher proportion of enstatite (> 10 vol% and up to ~30 vol%) at the expense of forsterite. It is noteworthy that some harzburgites identified at Koniambo and Nakéty contain diopside as an accessory phase (< 1 vol%), either overgrowing enstatite crystals or as a late interstitial phase. In lherzolite, proportions of enstatite and forsterite are about 45 vol% while the diopside content increases up to 5–10 vol% forming large, automorph crystals, as well as exsolutions within enstatite. Serpentinization, characterized by the formation of lizardite ± chrysotile at the expense of primary mantle silicates, is ubiquitous within the peridotite. In moderately (~30–50%) serpentinized peridotites (i.e. distal to the serpentine sole), lizardite occur mainly as a vein network (or mesh) fragmenting olivine and pyroxene crystals (Fig. 5A–I). Pervasive serpentinization of the fragmented silicates may be observed but rarely penetrates deep into the primary silicate crystals. In strongly serpentinized peridotites, such as the lherzolite-derived serpentinites typically observed in Tiébaghi, most if not all the primary silicates are pseudomorphologically replaced by lizardite after extensive, pervasive serpentinization (Fig. 5J–K). Serpentinization is commonly accompanied by the formation of magnetite, either along initial crystallographic planes of serpentinized enstatite or as euhedral crystals in serpentinized forsterite (Fig. 5K–L). Also, some calcite veins developed at the expense of diopside are locally observed in moderately serpentinized lherzolites (Fig. 5H). These veins, which are not recognized in highly serpentinized peridotites, probably formed early during the serpentinization process (i.e. prior to the complete serpentinization of the peridotite).

5.1.2. Major and trace element geochemistry

Eleven samples of unweathered peridotites including dunite, harzburgite, lherzolite and lherzolite-derived serpentinite were analyzed for whole-rock major and trace element geochemistry (online supplementary material). Also, six samples of unweathered lherzolite from the Babouillat zone of the Tiébaghi massif analyzed by Ulrich (2010) were included to this dataset. Silica, Mg and, to lesser extent, Fe are the principal constitutive elements in peridotites, with SiO_2, MgO and FeO concentrations of 38–43, 35–45 and 6–7 wt%, respectively (Fig. 6A). Whole-rock concentrations for major elements are consistent with the mineral chemistry of the principal constitutive phases (forsterite,

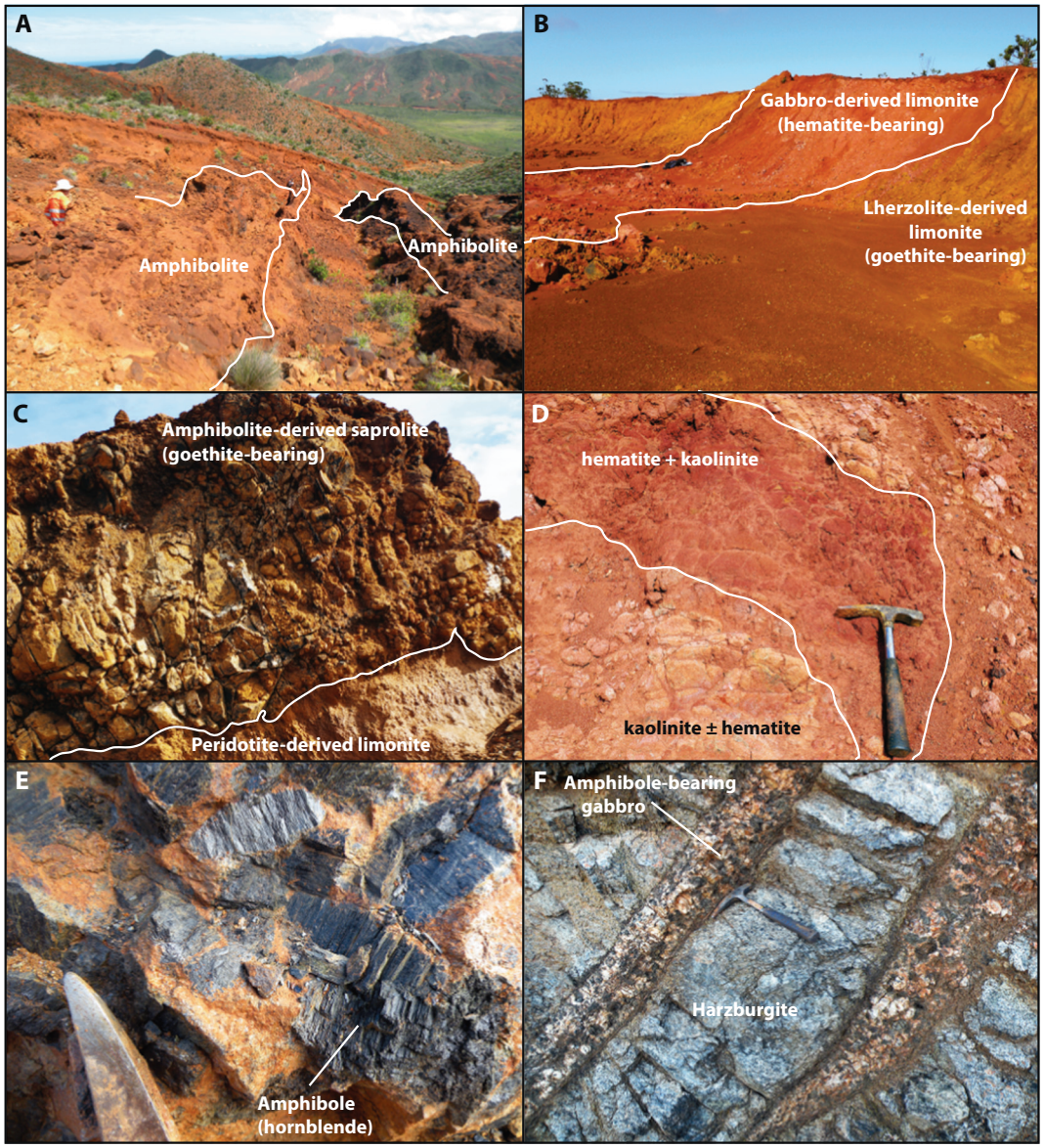

Fig. 4. Field photographs of amphibolite- and gabbro-derived laterites. (A) Weathered amphibolite dykes cutting across harzburgite-derived laterite. Exposed dykes form positive reliefs due to increased resistance to weathering (N'Go), (B) Hematite-bearing, gabbro-derived limonite cutting across lherzolite-derived limonite (Tiébaghi). (C) Goethite-bearing, saprolitized dyke of amphibolite overlying harzburgite- or dunite-derived limonite (N'Go), (D) Internal facies zonation within gabbro-derived saprolite exhibiting pale reddish zones dominated by kaolinite ± hematite and darker reddish zones with higher proportions of hematite (Tiébaghi), (E) Unweathered amphibolite containing amphibole (hornblende) porphyroblasts (N'Go), (F) Unweathered amphibole-bearing gabbro intrusions (Tiébaghi).

lizardite, enstatite) as analyzed by EPMA (Fig. 6A). Moderately serpentinized dunite and harzburgite yield the highest MgO content owing to higher proportion of Mg-rich forsterite. The elevated LOI illustrates the significant contribution of serpentine (lizardite) in peridotites, from about 6 wt% LOI in moderately serpentinized (~30% serpentine) peridotites to about 17 wt% in serpentinites (~100% serpentine). Al_2O_3 and CaO concentrations vary from about ~0.25 wt% in dunite to about 2 wt% in lherzolite (Fig. 6A) and are, therefore, inversely correlated with MgO. The Al_2O_3 content of peridotites mostly relates to the proportion of Al-bearing (1.6 to 3 wt% Al_2O_3) enstatite (Fig. 6A). The CaO content also largely relates to the proportion of enstatite (which contains up to 2 wt% CaO). Although accessory, Ca-rich diopside (~24 wt% CaO) may significantly contribute to the total CaO content of lherzolites. The Cr_2O_3 content of peridotites ranges from 0.3 to 0.5 wt% and results from the contribution of enstatite and accessory Cr-spinel. The Ni content ranges from 0.20 to 0.25 wt% with higher grades reached in harzburgite and dunite owing to higher proportion of Ni-bearing forsterite (0.25–0.40 wt% Ni).

Similar to Al, Sc exhibits large variations of concentration in peridotites, from 3–5 ppm in dunite to 6–8 ppm in harzburgite and 10–25 ppm in lherzolite (Fig. 6B). Lherzolites investigated in this study from the Alpha and Fantoche deposits (Tiébaghi) have relatively low Sc concentrations (~10 ppm) whereas lherzolites from the Babouillat zone (Tiébaghi) analyzed by Ulrich (2010) yield higher Sc concentrations (15–25 ppm). LA-ICP-MS analysis (Fig. 7) indicates that the Sc content in mantle silicates increases from forsterite (3–7 ppm) to enstatite (15–30 ppm) and diopside (40–70 ppm), so that the increase of the Sc content in peridotites from dunite to harzburgite and lherzolite relates to increasing proportions of enstatite (and accessorily diopside) at the expense of forsterite. The Sc content of enstatite and diopside may vary depending on the peridotite massif. Enstatite in dunite and harzburgite from the N'Go massif yields Sc content of 15–20 ppm, while enstatite in harzburgite from the Nakéty and Koniambo massifs yields Sc content of 20–30 ppm, and enstatite in lherzolite from the Tiébaghi massif yields

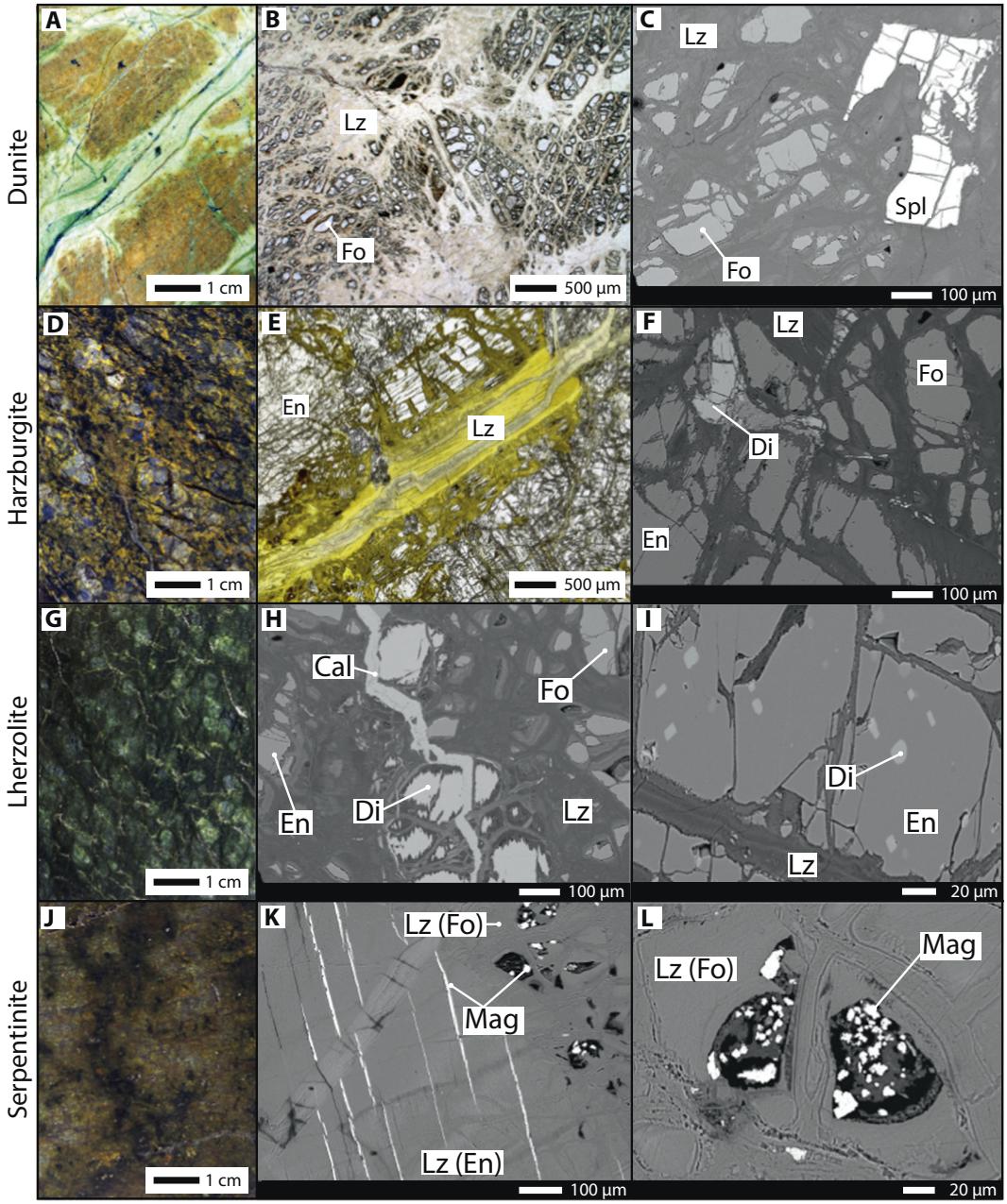

Fig. 5. Optic and SEM microphotographs of mineral assemblages in peridotitic bedrocks. (A–C) Dunite from Cap Bocage, (D–F) Harzburgite from Koniambo, (G–I) Lherzolite from Tiebaghi, (J–K) serpentinite from Tiébaghi. Mineral abbrev.: Lz = lizardite, Fo = forsterite, Spl = spinel, En = enstatite, Di = diopside, Cal = calcite, Lz(Fo) = lizardite after forsterite, Lz(En) = lizardite after enstatite, Mag = magnetite.

Sc content of ~30 ppm. Similarly, diopside in harzburgite from Koniambo yields Sc content of 40–50 ppm while diopside in harzburgite from Nakéty and in lherzolite from Tiébaghi yields Sc content of 60–70 ppm (Fig. 7). Sc concentrations in lizardite (5–50 ppm) strongly depend on the Sc content of the mantle silicate precursors and, therefore, cover most of the range observed in primary silicates (Fig. 7). The equivalence between the Sc content of lizardite and the Sc content of its silicate precursor, together with the lack of any correlation between whole-rock LOI (controlled by the relative amount of lizardite) and Sc concentrations (Fig. 6B), indicates that the degree of serpentinization does not affect the whole-rock Sc content of peridotites. This is in agreement with previous investigations on serpentinized peridotites (Orberger et al., 1995) wherein Sc is considered as inert during the serpentinization process and is used as a proxy to recalculate the initial (i.e. pre-serpentinization) diopside content of peridotites.

Whole-rock Sc concentrations are well correlated with V and to a lesser extent with Al concentrations (Fig. 6B), so that the whole-rock Sc content of peridotites may be approximatively estimated from the Al and V concentrations as following:

$$\mathrm{Sc\ (ppm)} = 10.6 * \mathrm{Al_2O_3\ (wt\%)} = 0.22 * \mathrm{V\ (ppm)} \quad (1)$$

These whole-rock correlations result from changes in the proportion and composition of enstatite and diopside (Fig. 7). In enstatite, Sc and Al concentrations define a trend from low-Al-Sc enstatite in N'Go and Cap Bocage dunite and harzburgite (3000–5000 ppm Al, 10–20 ppm Sc) to higher-Al-Sc-enstatite in Tiébaghi lherzolite (15,000–20,000 ppm Al, ~30 ppm Sc) with intermediate concentrations occurring in enstatite from Nakéty and Koniambo harzburgites. The positive correlation between Al and Sc in peridotites is therefore not only due to increasing proportions of enstatite at the expense of forsterite, but also to co-

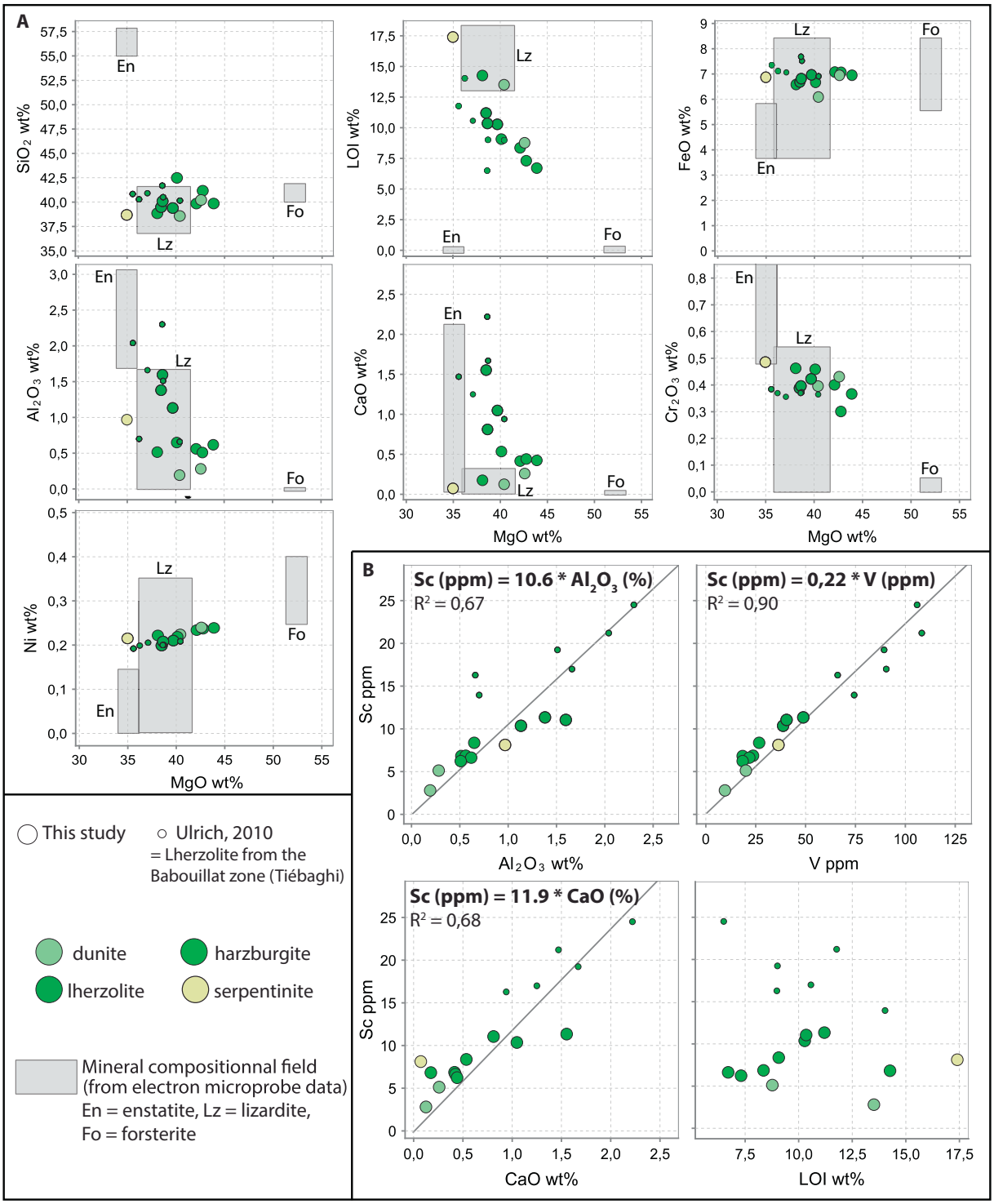

Fig. 6. Whole-rock geochemistry data for peridotites (dunite, harzburgite, lherzolite and serpentinite). (A) Plots of SiO_2, LOI, FeO, Al_2O_3, CaO, Cr_2O_3 and Ni (wt%) against MgO (wt%). Grey rectangles indicate mineral compositions from electron microprobe data. (B) Plots and correlations of Sc (ppm) against Al_2O_3 (wt%), V (ppm), CaO (wt%) and LOI (wt%).

increasing Al and Sc concentrations within enstatite from dunite and harzburgite facies of the southern massifs to harzburgite and lherzolite facies of the northern massifs. In Sc-rich lherzolite (> 15 ppm), enstatite alone can hardly account for the elevated Sc content. In such facies, diopside contributes significantly to the whole-rock Sc budget. Also, mineral chemistry data indicates that Sc and V concentrations co-increase from forsterite to enstatite and diopside, so that the Sc content of peridotitic mineral phases may be approximatively estimated from its V content as following:

$$\mathrm{Sc\ (ppm)} = 0.27 * \mathrm{V\ (ppm)} + 6.7 \quad (2)$$

Increasing proportions of Sc- and V-bearing enstatite and diopside in peridotites well explain the positive Sc–V correlation identified from whole-rock analysis (Figs. 6, 7). Eventually, Sc and Ti concentrations in primary silicates may exhibit correlation trends from low-Sc-Ti-forsterite to higher-Sc-Ti-enstatite and diopside. However, contrasting

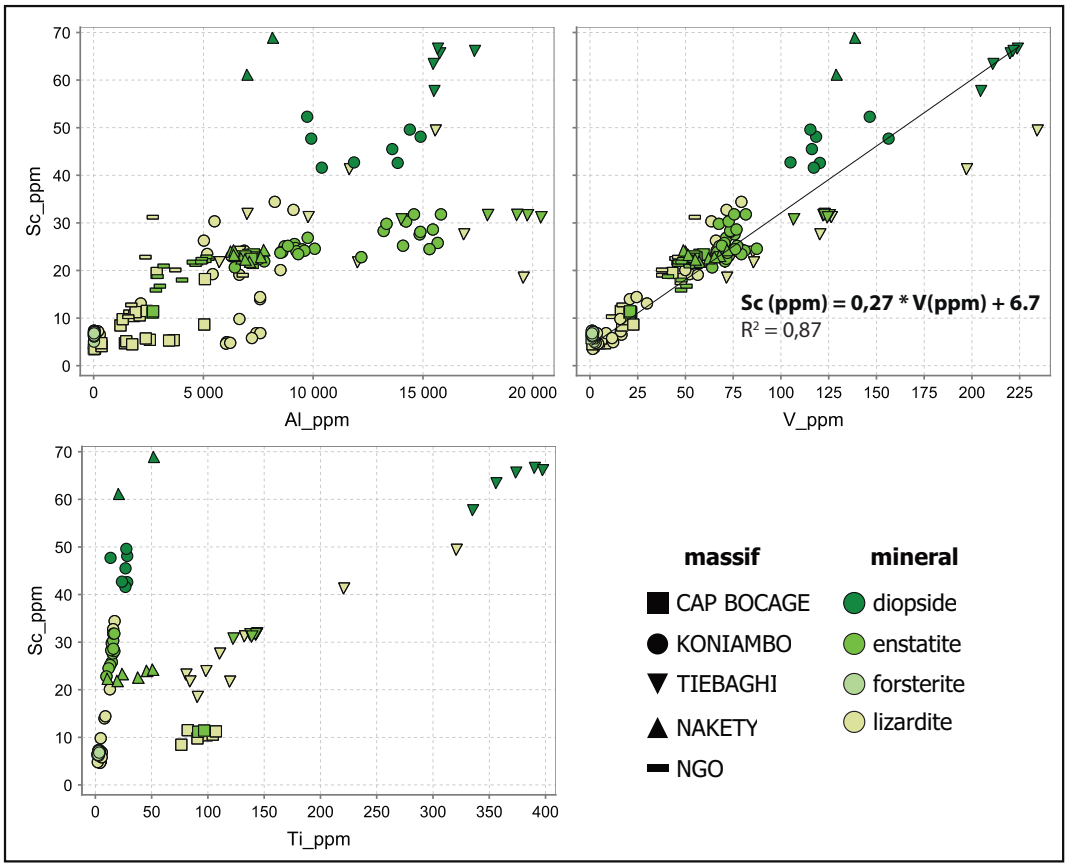

Fig. 7. Plots of Sc (ppm) against Al, V and Ti (ppm) in peridotitic minerals (diopside, enstatite, forsterite and lizardite) from LA-ICP-MS data.

with the Sc-Al and Sc-V correlations, the Sc-Ti correlation displays specific slopes depending on the peridotite massif, suggesting that Sc-Ti correlations may only be defined at the regional scale of the massif.

5.2. Mafic-ultramafic intrusive rocks

5.2.1. Mineral assemblages

Unweathered mafic-ultramafic intrusive rocks including amphibolite, amphibole-bearing pyroxenite and amphibole-bearing gabbro exhibit specific mineral assemblages and textures. Amphibolite occurrences identified in Nakéty and N'Go contain over 90 vol% hornblende with crystal size ranging from < 500 µm to ~10 cm together with minor enstatite and accessory titanite and Fe-Ti-oxides (Fig. 8A–C). Textural relationships indicate that hornblende develops surrounding corroded enstatite cores. Similar mineral assemblages are observed in amphibole-bearing pyroxenite although enstatite occurs in greater proportion from > 10 up to 80 vol% (Fig. 8C–E). Whereas hornblende may develop porphyroblastic textures with crystals up to 10 cm, enstatite crystal size rarely exceeds 5 mm. Amphibole-bearing gabbro and microgabbro from N'Go, Nakéty and Tiébaghi contain 50 to 90 vol% plagioclase and 10 to 50 vol% hornblende, together with accessory Fe-Ti oxides, sulfides and/or phosphates (Fig. 8G–L). As confirmed by mineral chemistry analysis (see below), plagioclase exhibit various composition ranging from anorthite to andesine. In all mafic-ultramafic dykes, secondary chlorite commonly forms at the expense of enstatite and plagioclase (Fig. 8L). Prehnitization of anorthite is also observed in some gabbro occurrences from Tiébaghi.

5.2.2. Major and trace element geochemistry

Twelve samples of unweathered amphibolite, amphibole-bearing pyroxenite and amphibole-bearing gabbro were analyzed for whole-rock major and trace element geochemistry (online supplementary material). Magnesium and Fe whole-rock contents are positively correlated with increasing FeO and MgO following the sequence amphibole-bearing gabbro (5–10 wt% MgO; 4–8 wt% FeO), amphibolite (15–20 wt% MgO; 9–11 wt% FeO) and amphibole-bearing pyroxenite (25 wt% MgO; 15 wt% FeO) (Fig. 9A). Conversely, Mg and Al whole-rock contents are inversely correlated as Al_2O_3 concentrations decrease from > 15 wt% in gabbro to 6–11 wt% in amphibolite and down to ~3 wt% in pyroxenite. These whole-rock relationships for major elements are well explained by varying proportions of the principal constitutive phases, as (i) Al-rich and Mg-Fe-free plagioclase is predominant in gabbro, (ii) Al-Fe-Mg-bearing hornblende is predominant in amphibolite and (iii) Al-poor and Mg-Fe-rich enstatite is predominant in pyroxenite. Similar to Al, Ca and Na whole-rock concentrations are broadly negatively related to Mg and decrease from amphibolite to pyroxenite owing to increasing proportion of Ca-Na-poor enstatite at the expense of Ca-Na-bearing hornblende. In gabbro, the Ca and Na whole-rock content may vary significantly depending both on the relative proportion of plagioclase and hornblende, and on the Ca/Na ratio of plagioclase. Titanium has a maximum concentration in amphibolite reaching up to 1.3 wt% TiO_2. Mineral chemistry analysis suggests that hornblende is the predominant carrier of Ti in amphibolite, although significant contribution of accessory titanite and/or Fe-Ti oxides to the whole-rock Ti budget is not excluded.

Similar to major elements, Sc exhibits large variations of concentration in mafic-ultramafic intrusive rocks, from 30–50 ppm in pyroxenite to 40–80 ppm in gabbro and 100–130 ppm in amphibolite (Fig. 9B). LA-ICP-MS analysis (Fig. 10) indicates that Sc is dominantly hosted by hornblende with Sc concentrations ranging from 50 to 180 ppm and to a lesser extent by enstatite (20–25 ppm), while other mineral phases (plagioclase, Fe-Ti oxides) yield low Sc concentrations (< 5 ppm). Therefore, the whole-rock Sc content of unweathered intrusive rocks depends both on the relative proportion and the Sc

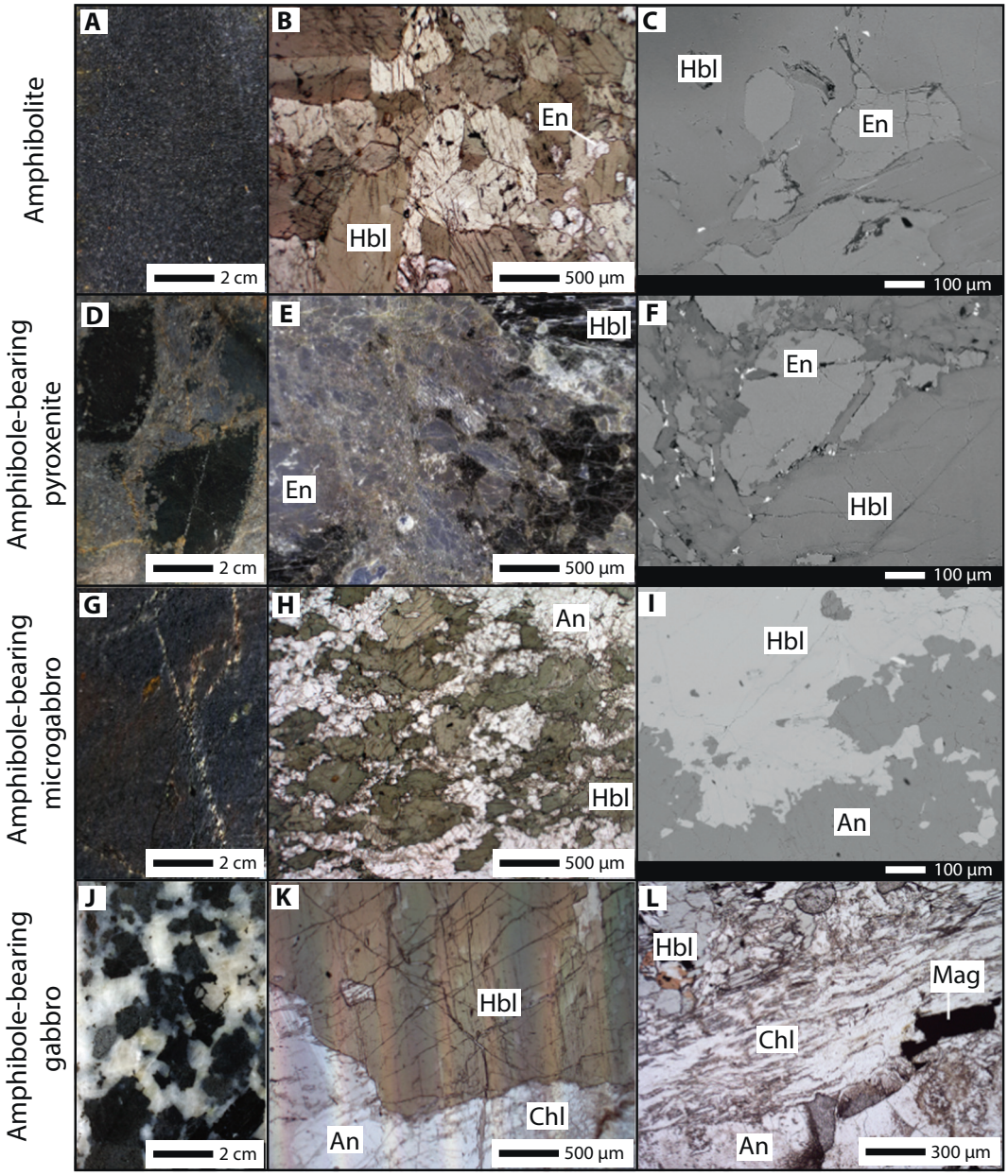

Fig. 8. Optic and SEM microphotographs of mineral assemblages in mafic intrusive bedrocks from N'Go, Nakéty and Tiébaghi. (A–C) Amphibolite, (D–F) Amphibole-bearing pyroxenite, (G–I) amphibole-bearing microgabbro, (J–K) amphibole-bearing gabbro. Mineral abbrev.: Hbl = hornblende, En = enstatite, An = anorthite, Chl = chlorite, Mag = magnetite.

content of hornblende. Noteworthily, amphibolite (> 90 vol% hornblende) typically contains Sc-rich hornblende (> 100 ppm), so that the whole-rock Sc content of amphibolite is correspondingly high. Sc-rich hornblende may also occur in gabbro and microgabbro as those identified in Nakéty and Tiébaghi, although the large proportion of Sc-poor plagioclase in gabbros dilutes and buffers the contribution of Sc-rich hornblende to the whole-rock Sc content. In contrast, hornblende-bearing pyroxenite, together with some other gabbro occurrences identified in N'Go, contain hornblende with a lower Sc content (50–80 ppm), so that the whole-rock Sc content of pyroxenite does not exceed 50 ppm despite containing a significant proportion of hornblende in the mineral assemblage.

Importantly, whole-rock Sc concentrations are well correlated with Ti and V concentrations (Fig. 9B), so that the Sc content of mafic-ultramafic intrusive rocks may be estimated from the Ti and V concentrations as following:

$$\mathrm{Sc\ (ppm)} = 98 * \mathrm{TiO_2\ (wt\%)} = 0.17 * \mathrm{V\ (ppm)} \quad (3)$$

As revealed by mineral chemistry analysis (Fig. 10), these whole-rock correlation trends are best explained by the co-variation of the Sc, V and Ti contents of hornblende, which is the predominant mineral host for these elements. At the mineral scale, the Sc content of hornblende may be estimated from the Ti, V but also the Fe contents of hornblende, as following:

$$\mathrm{Sc\ (ppm)} = 0.016 * \mathrm{Ti\ (ppm)} = 0.15 * \mathrm{V\ (ppm)} = 157 * \mathrm{Fe\ (wt\%)} \quad (4)$$

whereas Sc, Ti and V are predominantly hosted by hornblende so that their positive correlation in hornblende directly translates into whole-rock correlation trends, Fe is hosted both by hornblende and enstatite, and the whole-rock Fe content cannot be indicative of the Sc content except for monomineralic amphibolite.

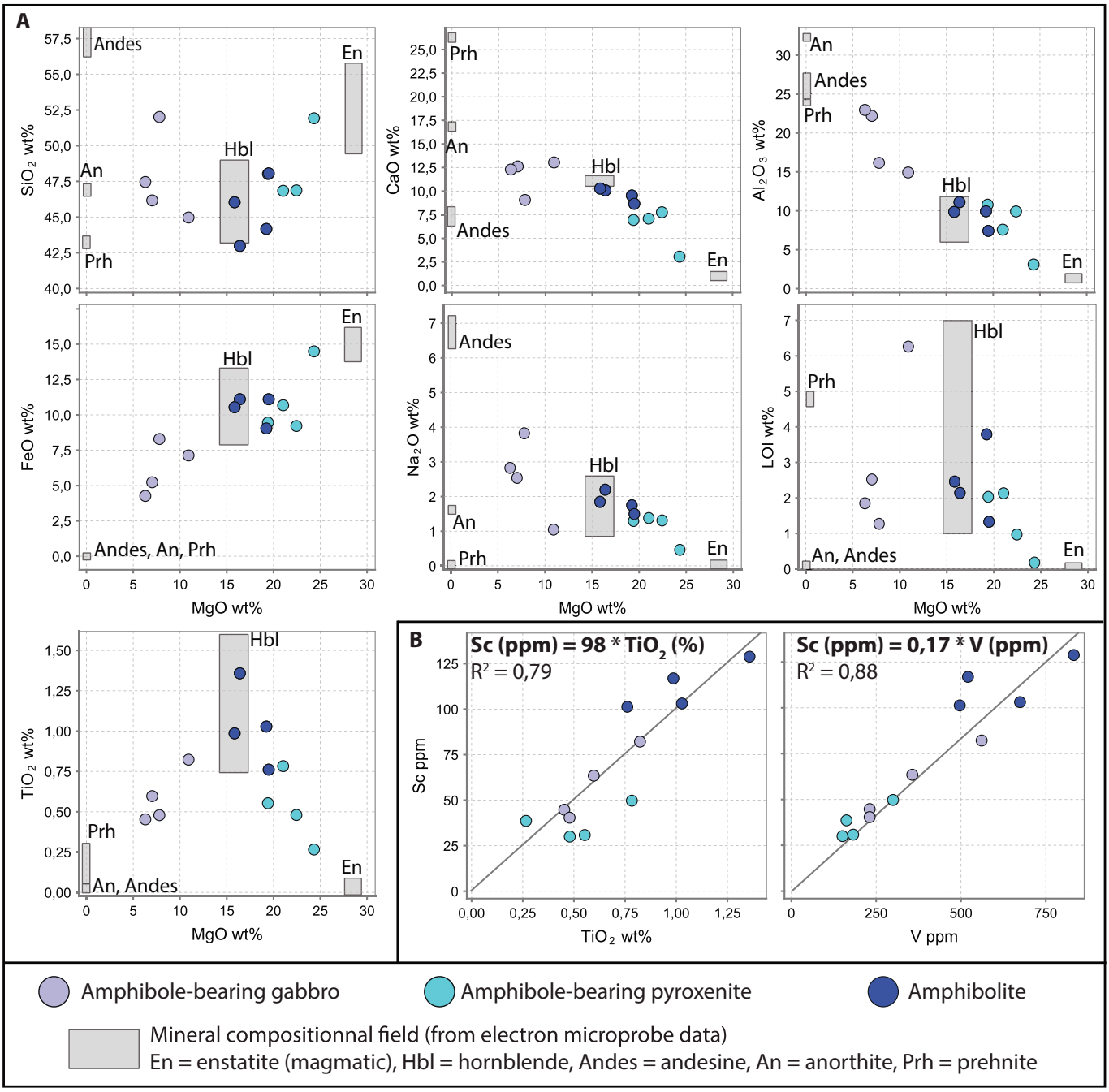

Fig. 9. Whole-rock geochemistry data for mafic-ultramafic intrusive rocks (amphibole-bearing gabbro, amphibole-bearing pyroxenite, amphibolite). (A) Plots of SiO_2, CaO, Al_2O_3, FeO, Na_2O, LOI and TiO_2 (wt%) against MgO (wt%). Grey rectangles indicate mineral compositions from electron microprobe data. (B) Plots and correlations of Sc (ppm) against TiO_2 (wt%) and V (ppm).

6. Scandium in laterites

6.1. Peridotite-hosted Ni-Co laterites

6.1.1. Paragenetic sequence

Lateritization of peridotites is characterized by the development of several alteration facies from the bedrock to the ferricrete and is associated with complex mineral and textural transformations (Fig. 11). The paragenetic sequence commonly observed in peridotite-derived laterite typically includes multiple stages of hydration and dissolution of primary silicates and formation of secondary silicates and oxides-oxyhydroxides (Fig. 12). At the bedrock – saprock interface, hydrolysis and dissolution - repecipitation of mantle silicates (olivine, pyroxene) is associated with the development of secondary goethite (referred to as skeletal goethite, Go-sk) along silicate grain boundaries and crystallographic planes (Fig. 11A–C). Lizardite (Lz) is preserved from dissolution in the saprock although it is largely transformed into secondary, nickeliferous serpentine/talc-like (Lz-ni) either along fractures (Fig. 11A) or through pervasive replacement (Fig. 11B, C). Locally, accessory quartz and/or smectites may form as infills of pre-existing silicates (Fig. 11C), but these are in turn rapidly dissolved upwards in the sequence. Some atypical clay-rich laterite such as those developed at Tiébaghi exhibit well-developed smectitic zones mostly consisting of Ni-bearing nontronite pseudomorphing primary silicates (Fig. 11D). However, in most investigated profiles elsewhere in New Caledonia, the saprock directly grades upwards into the saprolite wherein most

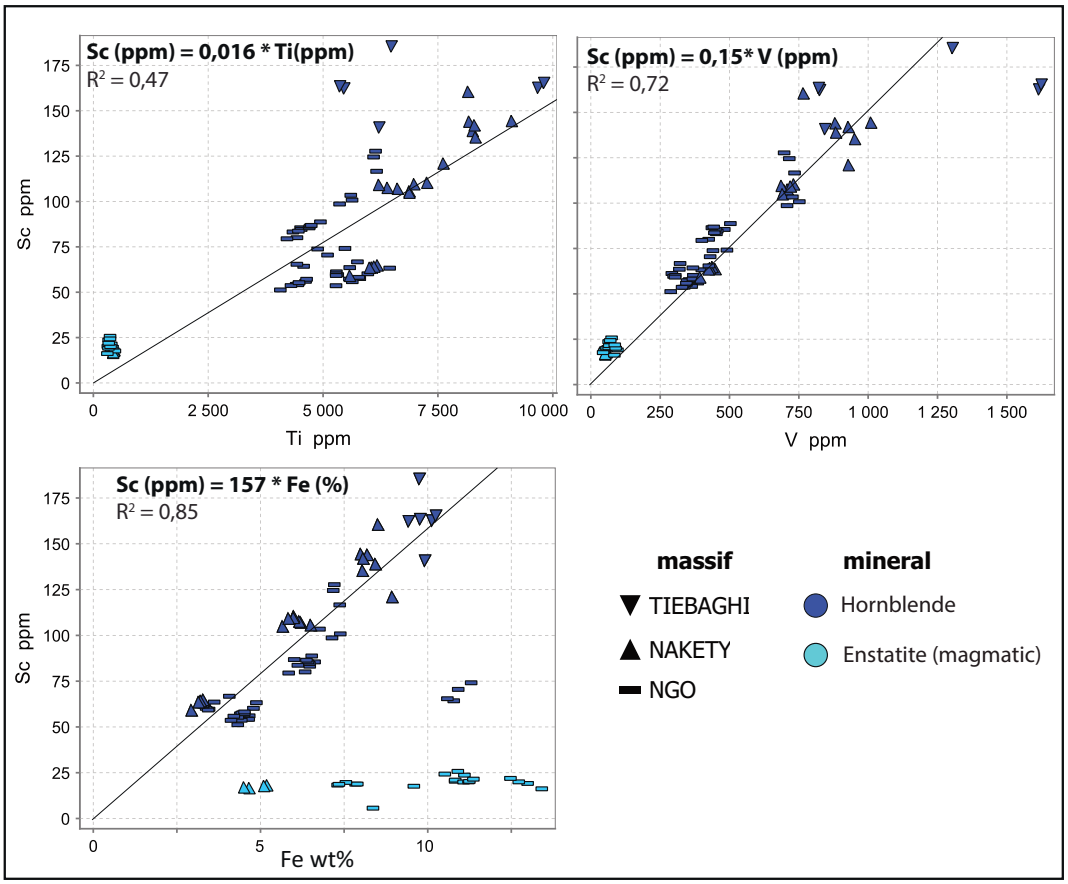

Fig. 10. Plots and correlations of Sc (ppm) against Ti, V (ppm) and Fe (wt%) in magmatic minerals (enstatite and hornblende) from LA-ICP-MS data.

(> 80 vol%) of the primary and secondary serpentines are epigenized into goethite (Gth-lz) (Fig. 11E). Fine-grained goethitic material derived from the overlying limonite (Gth-lt) may occur as physical infill of voids and notably within dissolved/skeletized silicates (Fig. 11F). The transition zone between the saprolite and the limonite is marked by the accumulation (up to ~5 vol%) of Mn-Co-Ni oxides mostly represented by lithiophorite (Lhpi) which develops at the expense of epigenetic goethite Gth-lz (Fig. 11G). Upwards, the yellow limonite is characterized by the progressive compaction and destruction of pre-existing structures through the fragmentation of skeletal (Gth-sk) and epigenetic (Gth-lz) goethite (Fig. 11H). These fragments are loosely cemented by fine grained, limonitic (i.e. ochreous) goethite (Gth-lt) that likely underwent several stages of fragmentation, dissolution and reprecipitation (Fig. 11I). The transition from the yellow to the red limonite is associated with the formation of accessory, fine grained hematite (Hem-lt) at the expense of the ochreous goethite matrix (Gth-lt), together with the progressive decrease in size and abundance of the remaining skeletal/epigenetic goethite and Mn-Co-Ni oxide clasts (Fig. 11J). Eventually, the red limonite is capped by the ferruginous hardcap or ferricrete. The basal portion of the ferricrete is usually autochtonous and is characterized by the crystallization of euhedral goethite (Gth-fe, up to ~5 μm) and hematite (Hem-fe, up to 1 μm) at the expense of pre-existing oxides (Fig. 11K). The upper portion of the ferricrete usually consists of accumulated goethitic and hematitic pisoliths (Gth-pi and Hem-pi) cemented by a goethite-rich matrix (Fig. 11L). Overgrowth of pisolithic goethite on hematite cortex is commonly observed. Also, large (3 mm–1 cm) goethite pisoliths may exhibit zonation textures indicating successive growth stages. Throughout the lateritic profile, accessory magnetite and chromiferous spinel are mostly resistant to weathering and residually accumulate upwards.

6.1.2. *Distribution of major and trace elements*

The present section first describes the whole-rock geochemical changes along three profiles selected for their representativeness: (i) the dunite-derived PZ1B profile (17 samples) from Cap Bocage (Fig. 13), (ii) the harzburgite-derived OPB7 profile (16 samples) from Koniambo (Fig. 14) and (iii) the lherzolite-derived TIEA profile (14 samples) from Tiébaghi (Fig. 15). Elementary correlations obtained from whole-rock analysis (Fig. 16) are then presented for the entire dataset that includes 104 samples collected along fourteen peridotite-derived lateritic profiles (online supplementary material). In situ minor (Si, Al, Cr, Ni; EPMA WDS analysis) and trace (Sc; LA-ICP-MS analysis) element concentrations in goethite, hematite and lithiophorite along the OPB7 profile are finally documented (Fig. 17) and discussed with regards to whole-rock geochemical data.

Typical oxide-rich lateritic profiles PZ1B and OPB7 exhibit characteristic geochemical distribution patterns. In both profiles, the saprock to saprolite interface constitutes the most prominent geochemical transition with the sharp depletion of SiO_2 and MgO from 40 to < 5–10 wt%, and the concomitant increase in Fe_2O_3 from ~7 to ~60 wt% (Figs. 13, 14). Contrasting with oxide-rich laterites, lateritic profiles from Tiébaghi exhibit clay-rich saprolitic zones characterized by more progressive Mg depletion and Fe enrichment (Fig. 15). From the base of the saprolite up to the ferricrete, Fe_2O_3 concentrations increase to ~70 wt% together with further decrease of the SiO_2 and MgO contents. Similar to Fe, a number of elements including Al, Cr, Mn, Ni, Co, Sc, V and REEs exhibit a ~tenfold enrichment in the lateritic profile compared to the parent peridotite. However most of these elements display different distribution patterns compared to Fe in that their maximum concentrations occur at intermediate positions within the lateritic profile. Nickel usually reaches maximum concentrations in the saprock (~2 wt%) and almost linearly decreases in concentration upwards in

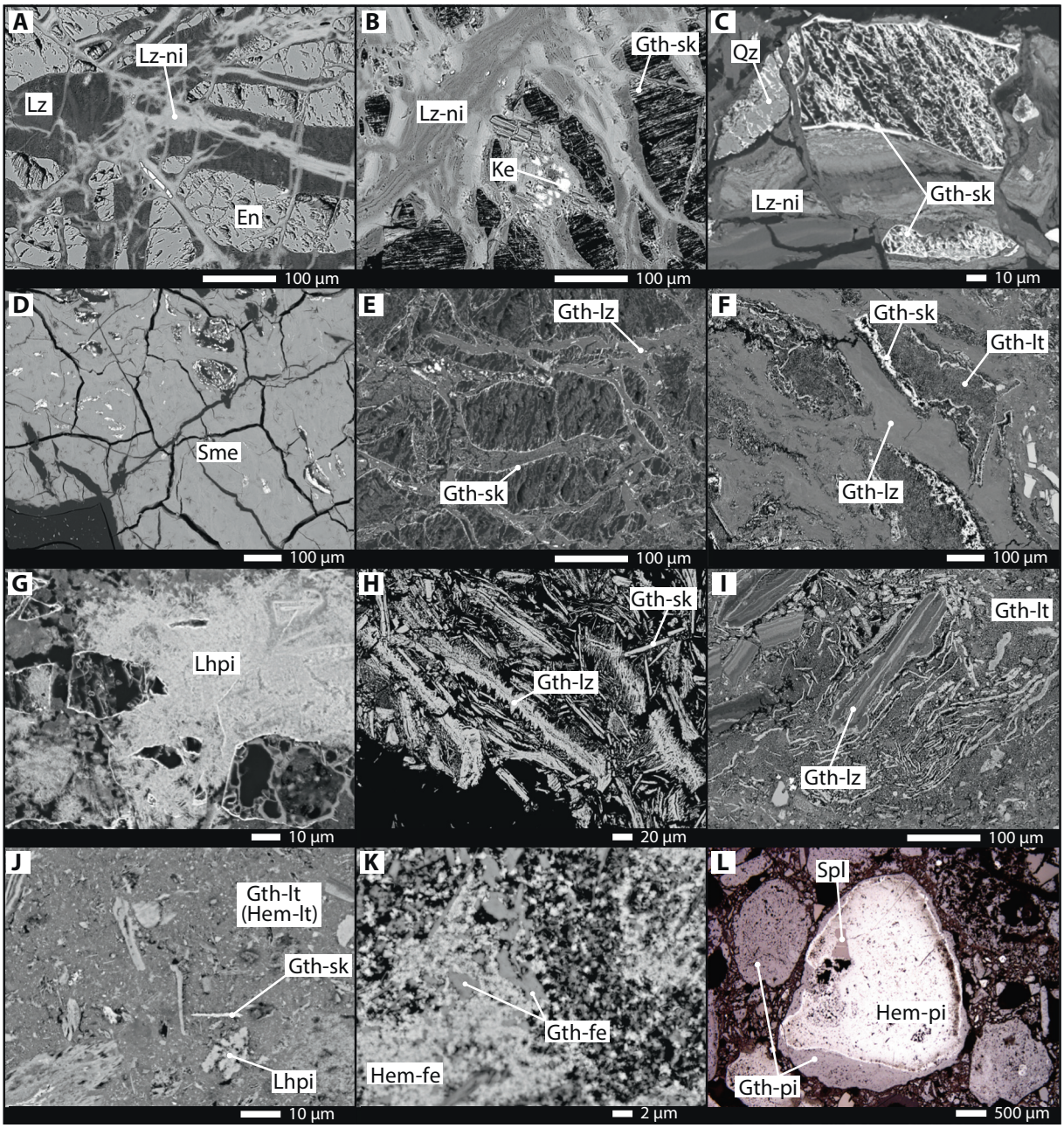

Fig. 11. Backscattered Electron (BSE) microphotographs: (A) Bedrock – saprock interface: onset of olivine/pyroxene dissolution and formation of secondary Ni-bearing serpentine/talc-like (Lz-ni) at the expense of lizardite (Lz). (B–C) Saprock: effective dissolution of olivine/pyroxene, formation of skeletal goethite (Gth-sk) preserving the structure of primary silicates, together with secondary Ni-bearing serpentine/talc-like (Lz-ni) and kerolite (Ke). (D) Smectite-rich zone from Tiébaghi laterites: replacement of primary and secondary serpentines by smectites (Sme), mostly Ni-bearing nontronite. (E–F) Saprolite: isovolumetric epigenization of serpentines into goethite (Gth-lz) and onset of void infill by fine-grained limonitic (ochreous) goethite (Gth-lt). (G) Transition zone: accumulation of Mn-Co-Ni oxides, mostly lithiophorite. (H–I) Yellow limonite: fragmentation of pre-existing structures. (J) Red limonite: Advanced texture obliteration, decrease in size and abundance of the goethite and Mn-oxide clasts, and formation of hematite (Hem-lt) within the goethite (Gth-lt) matrix. (K) Basal allochtonous ferricrete: formation of crystallized goethite (Gth-fe) and hematite (Hem-fe). (L) Pisolithic horizon: formation of pisolithic and nodular goethite (Gth-pi) locally overgrowing pisolithic hematite (Hem-pi) and/or encapsulating Cr-spinel (Spl) relics.

the profile, while Mn and Co concentrations are highest in the transition zone and decrease upwards. Contrastingly, Al and Sc concentrations progressively increase to reach a maximum in the yellow limonite and progressively decrease in the uppermost red limonite and ferricrete horizons (Figs. 13, 14). The initial Sc content of the parent peridotite strongly controls the maximum Sc grade of its lateritized derivatives, so that the dunite-derived yellow limonite from the PZ1B profile yields a maximum Sc grade of ~60 ppm, while the harzburgite- and lherzolite-derived yellow limonite from the OPB7 and TIEA profiles, respectively, yield maximum Sc grades of ~100 ppm.

The plot of Sc against Fe_2O_3 concentrations for the nine investigated lateritic profiles (Fig. 16A) indicates a positive correlation from the parent rock up to the lower portion of the saprolite ($Fe_2O_3 \leq 60$ wt%). There, the Sc content may be approximatively estimated from the Fe_2O_3 concentrations as following:

$$\mathrm{Sc\ (ppm)} = 0.99 * \mathrm{Fe_2O_3\ (wt\%)} \quad (5)$$

Above in the profiles ($Fe_2O_3 > 60$ wt%), Sc concentrations are

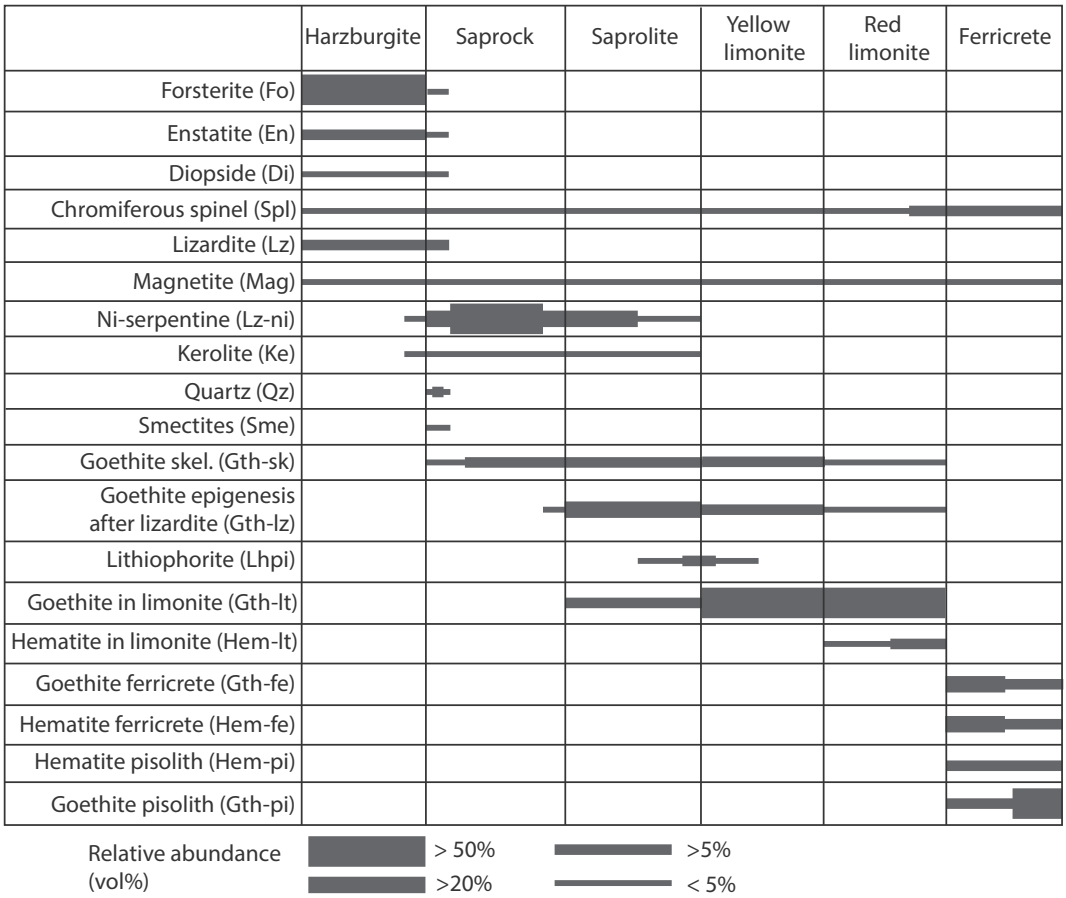

Fig. 12. Evolution of mineral relative abundances and assemblages along a typical lateritic sequence developed after harzburgite.

largely variable and discorrelated with Fe concentrations. From the upper portion of the saprolite up to the yellow limonite, Sc is presumably enriched compared to Fe, so that Sc grades reach 90–100 ppm in harzburgite- and lherzolite-derived laterites while the Fe_2O_3 content does not exceed 70 wt%. Scandium is negatively correlated to Fe in the uppermost horizons (red limonite and ferricrete), which are characterized by further Fe_2O_3 increase up to 80 wt% and Sc decrease down to ~10 ppm. In contrast, Sc concentrations are positively correlated with Al and to a lesser extent with V concentrations from the parent bedrock up the red limonite, so that the Sc content may be estimated from the Al_2O_3 and V concentrations as following:

$$Sc\ (ppm) = 11.2*Al_2O_3\ (wt\%) = 0.33*V\ (ppm) \quad (6)$$

In all profiles, most ferricrete samples are markedly out of the Fe_2O_3-Sc, Al_2O_3-Sc and V-Sc correlation trends. Such offsets from the correlations possibly relate to the contribution of allochtonous material in the ferricrete samples. These were, therefore, not taken into account in the correlations. In addition, the documented correlations do not include lateritic samples derived from peridotites when these were collected at proximity (< 3 m) to intrusive rocks.

At the mineral scale, in situ analyses of iron oxides and oxyhydroxides from the OPB7 profile reveal that the different generations of goethite and hematite (defined from optical and scanning electron microscopy, see Section 6.1.1) yield specific minor and trace element concentrations. Early-formed skeletal goethite yields the highest Si and Ni concentrations (~2 and 1 wt%, respectively) together with low Al and Cr concentrations (~1 and 0.3 wt%, respectively) (Fig. 17A). Subsequent formation of epigenetic and limonitic goethite is associated with a decrease in Si and Ni concentrations and an increase in Al and Cr concentrations. Late-stage ferricritic and pisolithic goethite and hematite are characterized by further depletion of Si and Ni, together with a major increase of the Cr content (up to 5 wt%) and variable Al concentrations. Also, as revealed by LA-ICP-MS analysis, in situ Sc concentrations of goethite and hematite strongly depends on their vertical position along the lateritic profile (Fig. 17B). In the OPB7 profile, the Sc content of goethite varies from ~60 ± 10 ppm at the base of the saprolite, up to 100 ± 25 ppm in the yellow limonite, and down to 25 ± 20 ppm in the pisolithes. Variations of Sc concentration in goethite, and to a lesser extent in hematite, largely explain the distribution of whole-rock Sc concentrations, so that the distribution of Sc in the laterite profile is mostly controlled by variations of the Sc content of goethite, rather than by the relative proportion of goethite and hematite. LA-ICP-MS analysis of accessory lithiophorite (Lhpi) in the saprolite suggests that Mn-oxides yield similar or slightly lower Sc concentrations compared to goethite and, therefore, marginal contribute to the Sc content of whole-rock samples.

6.2. Mafic-ultramafic intrusive rocks

6.2.1. Paragenetic sequence

Weathering of mafic and ultramafic intrusive rocks (amphibolites, pyroxenites and gabbros) results in the hydrolysis and dissolution of primary magmatic minerals and the formation of specific secondary mineral assemblages. In amphibolites and amphibole-bearing pyroxenites, dissolution of hornblende commonly initiates along crystallographic planes and is associated with the formation of early-stage skeletal goethite. Skeletal goethite networks are in turn coated either by euhedral gibbsite (Fig. 18A) or by poorly crystallized kaolinite (Fig. 18B), each individual goethitic compartment exhibiting either gibbsite or kaolinite coatings, but not both. Locally, exceptions occur and gibbsite may be present together with kaolinite within a single compartment. In such a case, textural relationships are unclear

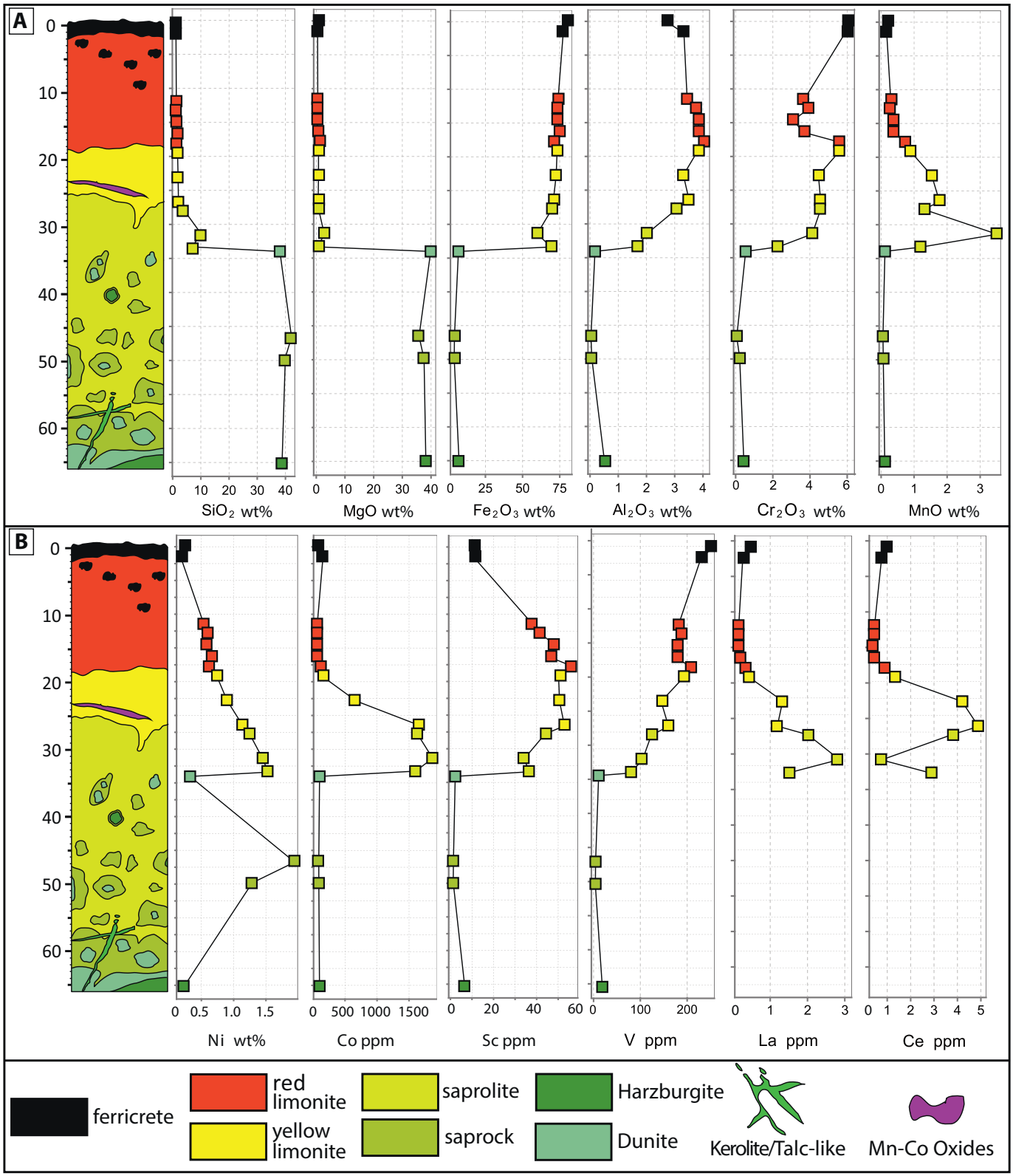

Fig. 13. Geochemical evolution along dunite-derived lateritic profile PZ1B (Cap Bocage): (A) Major oxides: SiO_2, MgO, Fe_2O_3, Al_2O_3, Cr_2O_3, MnO (wt%), (B) Economic elements: Ni (wt%), Co (ppm), Sc (ppm), trace and LREE: V, La, Ce (ppm).

although they suggest latter formation of gibbsite relative to kaolinite (Fig. 18E, F). Early-stage alteration of enstatite may result in the formation of smectites (Fig. 18C), which are in turn readily transformed into kaolinite (Fig. 18G). Further development of alteration leads to increased development of goethite at the expense of kaolinite (Fig. 18E, H), eventually resulting in the formation of a matured, goethite + gibbsite assemblage (Fig. 18I). Contrasting with amphibolites and pyroxenites, weathering of gabbro commonly results in the formation of kaolinite rather than Al-oxides (Fig. 18J), and, more importantly, the formation of hematite instead of goethite (Fig. 18K, L).

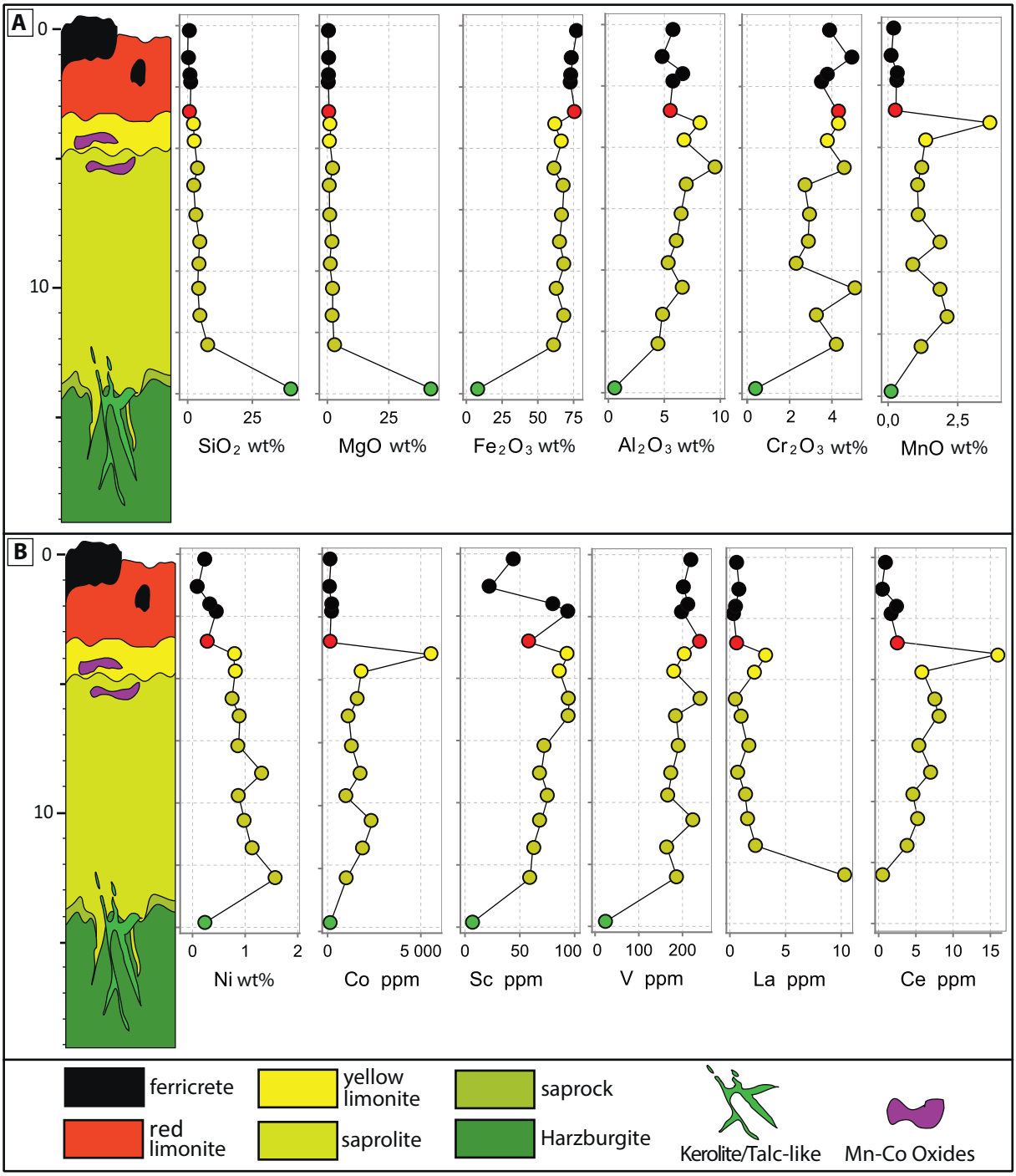

Fig. 14. Geochemical evolution along harzburgite-derived lateritic profile OPB7 (Koniambo): (A) Major oxides: SiO_2, MgO, Fe_2O_3, Al_2O_3, Cr_2O_3, MnO (wt%), (B) Economic elements: Ni (wt%), Co (ppm), Sc (ppm), trace and LREE: V, La, Ce (ppm).

There, hematite typically postdates kaolinite, as indicated by overgrowth (Fig. 18K) and replacement (Fig. 18L) textures. Such replacement of kaolinite by hematite argues for the downward remobilization of iron, as previously characterized in some African lateritic profiles (Ambrosi et al., 1986).

6.2.2. Distribution of major and trace elements

The saprolitization of amphibolite (and amphibole-bearing pyroxenite) dykes is associated with major depletion of mobile cations Si, Mg and Ca, together with the residual enrichment of Fe, Al and Cr (Fig. 19A). Owing to the formation and relative preservation of kaolinite in saprolitized amphibolites, the observed depletion in Si is progressive and delayed compared to the sharp depletion in Mg (and Ca), contrasting with typical peridotite-derived laterites wherein both Si and Mg exhibit sharp and congruent depletion. Fe and Cr enrichments are maximal at the top of the weathering profile, whereas Al concentrations are maximal at an intermediate position within the profile. Such distribution patterns are similar to those observed in typical peridotite-derived laterites. Economic elements Ni, Co and Sc also exhibit similar distribution patterns compared to those observed in Ni laterites. In the amphibolite-derived, saprolitic profile, Ni concentrations are maximum at the base of the saprolitized amphibolite although

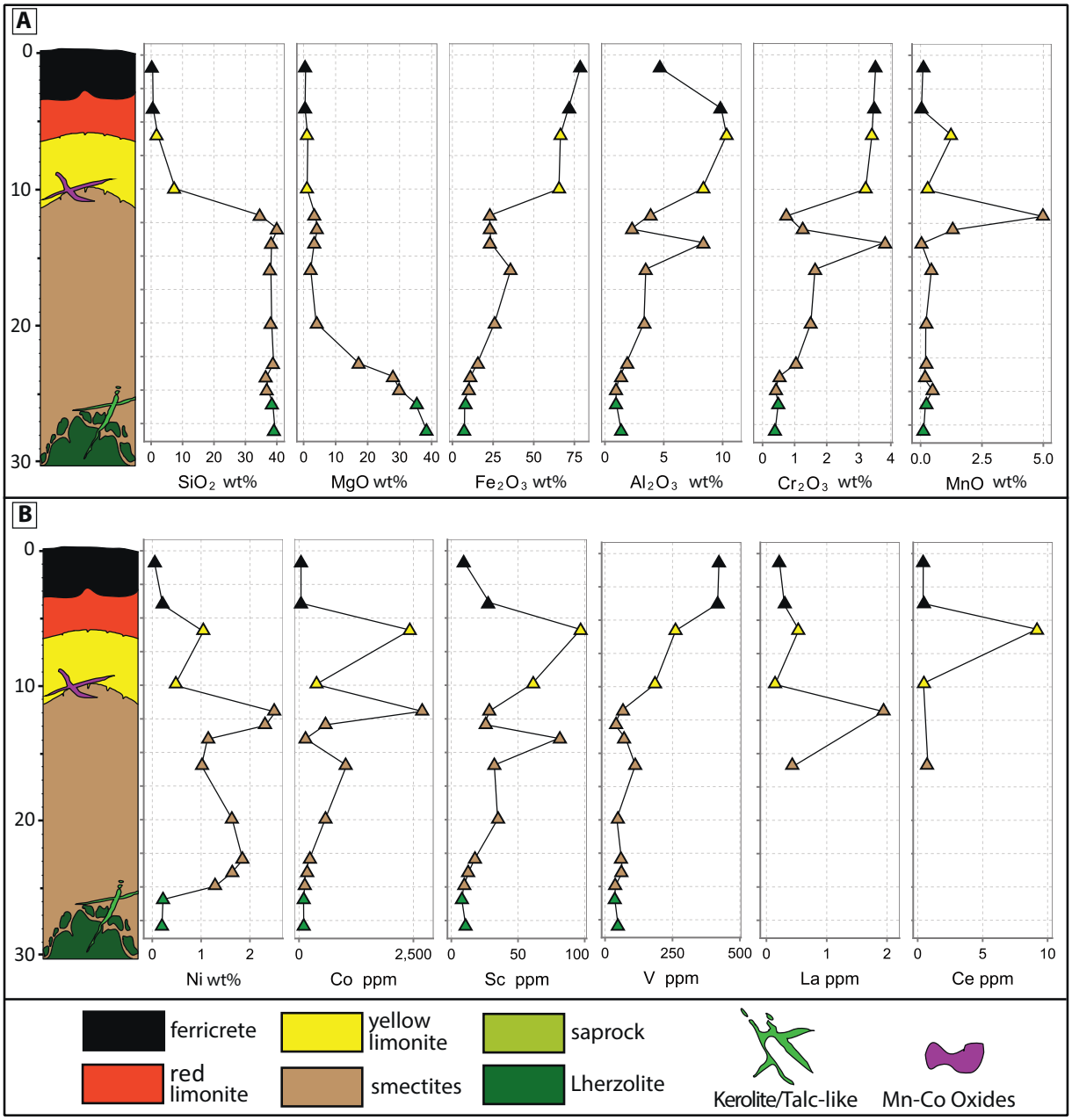

Fig. 15. Geochemical evolution along lherzolite-derived lateritic profile TIEA (Tiébaghi): (A) Major oxides: SiO_2, MgO, Fe_2O_3, Al_2O_3, Cr_2O_3, MnO (wt%), (B) Economic elements: Ni (wt%), Co (ppm), Sc (ppm), trace and LREE: V, La, Ce (ppm).

not exceeding 1 wt%. Cobalt and Sc maximum concentrations occur at intermediate position within the profile (Fig. 19B). Importantly, saprolitized amphibolites exhibit a two- to threefold increase in Sc concentrations compared to the parent rock, so that fertile amphibolites (≥100 ppm Sc) alter to saprolite with Sc concentrations up to ~200–300 ppm. As observed in Ni laterites, Sc in saprolitized amphibolites exhibit distribution patterns similar to those of Al and V.

At the mineral scale, WDS elementary mapping of mineral assemblages in saprolitized amphibolites indicate that Sc is essentially hosted by early-stage skeletal goethite and late-stage goethite formed after kaolinite, and to a much lesser extent by kaolinite (Fig. 20). In saprolites developed after fertile (> 100 ppm Sc) amphibolites, goethite yields Sc concentrations up to about 0.08 wt% (i.e. 800 ppm) together with Ni and Co concentrations up to 1 and 0.03 wt%, respectively. There, the spatial distribution of V appears similar to that of Sc. In contrast, Ti is mostly hosted by early-formed skeletal goethite and is largely absent in late-stage patchy goethite formed after kaolinite. It is noteworthy that the most-enriched sample with regards to its whole-rock Sc content (314 ppm) also contains non-negligible amounts of Mn (~1 wt%) and Co (~1000 ppm) owing to accessory (< 5 wt%) Mn-oxides (Fig. 19). There, a potential contribution of Mn-oxides to the global Sc budget cannot be excluded, although it would require extremely high Sc concentrations (> 1 wt%) in Mn-oxides. In this sample, the relative proportion of goethite (~40 wt%; based on mineral and whole-rock Fe concentrations), together with the average Sc content of goethite (~800 ppm), argue against any significant contribution of Mn-oxides to the whole-rock Sc content, as goethite alone can account for the global Sc budget. This is in agreement with the analysis of Mn-oxides in peridotite-derived laterites (see Fig. 17), which indicates that the Sc content of accessory Mn-oxides is similar to slightly lower compared to their goethitic matrix.

Contrasting with goethite-bearing saprolitized amphibolites,

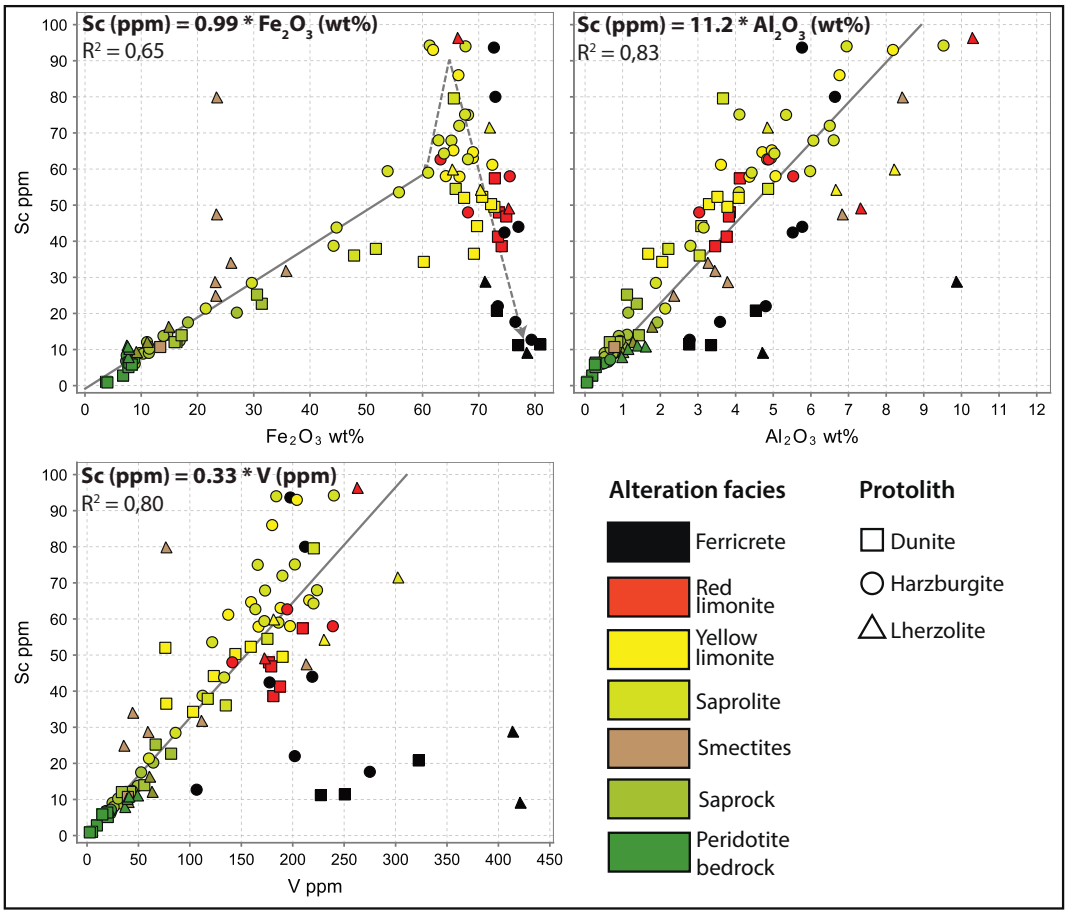

Fig. 16. Plots of Sc (ppm) as a function of Fe_2O_3, Al_2O_3 (wt%) and V (ppm) along the 9 investigated peridotite-derived lateritic profiles (whole-rock data).

hematite-bearing laterites developed after gabbros exhibit relatively low (usually < 50 ppm) whole-rock Sc concentrations (Fig. 21), i.e. lower than their unweathered counterparts (40–80 ppm, see Fig. 9 Section 5.2.2), suggesting the expulsion of during the weathering of gabbros. Such remobilization of Sc from gabbros is supported by the anomalously elevated Sc concentrations measured in footwall peridotite-derived limonite where the Sc content exceeds 150–200 ppm (Fig. 21). There, the observed Sc over-enrichment extends down to ~2 m below the base of the gabbro intrusive bodies.

7. Discussion and implications for Sc exploration

This study aims to document the distribution of Sc in New Caledonian laterites and to assess the main factors controlling its distribution in lateritic profiles that encompass the diversity of protoliths and alteration styles. Critical conditions for the development of Sc-rich zones with potential economic interest are discussed in the following section based on field and analytical investigations.

7.1. Preliminary genetic model and critical controls for the formation of Sc-rich laterites

Field and analytical data documented in the present contribution reveals a remarkable evolution of the Sc mineral hosts and abundances in lateritic profiles of New Caledonia, forming the basis of a genetic model for the enrichment of Sc in laterites developed after mafic and ultramafic rocks. In peridotite-derived lateritic profiles, the dissolution of primary silicates and leaching of Si and Mg lead to the co-enrichment of Sc with other poorly mobile elements, most notably Fe. From the bedrock to the saprolite, Sc concentrations co-increase with Fe concentrations, suggesting that Sc enrichment in the lower part of the laterite profile is essentially residual. Contrastingly, Sc commonly exhibits a relative enrichment compared to Fe in the yellow limonite and a relative depletion in the red limonite and ferricrete. Such a distribution pattern, similar to that of Al, supports a certain mobility of Sc, which is, to some extent, leached from the uppermost horizons (upper red limonite and ferricrete) and accumulated downwards in the yellow limonite. From the saprolite to the ferricrete, such variations in whole-rock Sc concentrations are primarily controlled by variations in the Sc content of goethite. The remobilization of Sc from the uppermost horizons is here interpreted to result from the release of Sc after (i) dissolution/recrystallization of goethite and (ii) from the formation of hematite at the expense of goethite. Repeated dissolution/recrystallization of goethite during the maturation of the lateritic profile leads to the formation of increasingly crystallized goethite (Dublet et al., 2015). This process is known to provoke release and downward remobilization of Ni from goethite in lateritic profiles (Dublet et al., 2015). Such model appears partly suitable for explaining the remobilization of Sc and its maximum enrichment in the yellow limonite, providing that downward-remobilized Sc from the uppermost horizons (red limonite and ferricrete) is more readily trapped in the directly underlying yellow limonite. In addition, the development of hematite at the expense of goethite likely participates in the remobilization of Sc from the red limonite and ferricrete, as Sc concentrations are commonly lower in hematite than in goethite. Such a behavior is similar to that of Al and Ni, which are known to substitute more easily for Fe in goethite than in hematite (Schwertmann and Latham, 1986; Trolard et al., 1995). However, red limonite commonly contains only accessory amounts of hematite, so that the formation of hematite at the expense of goethite is probably not the dominant process responsible for the

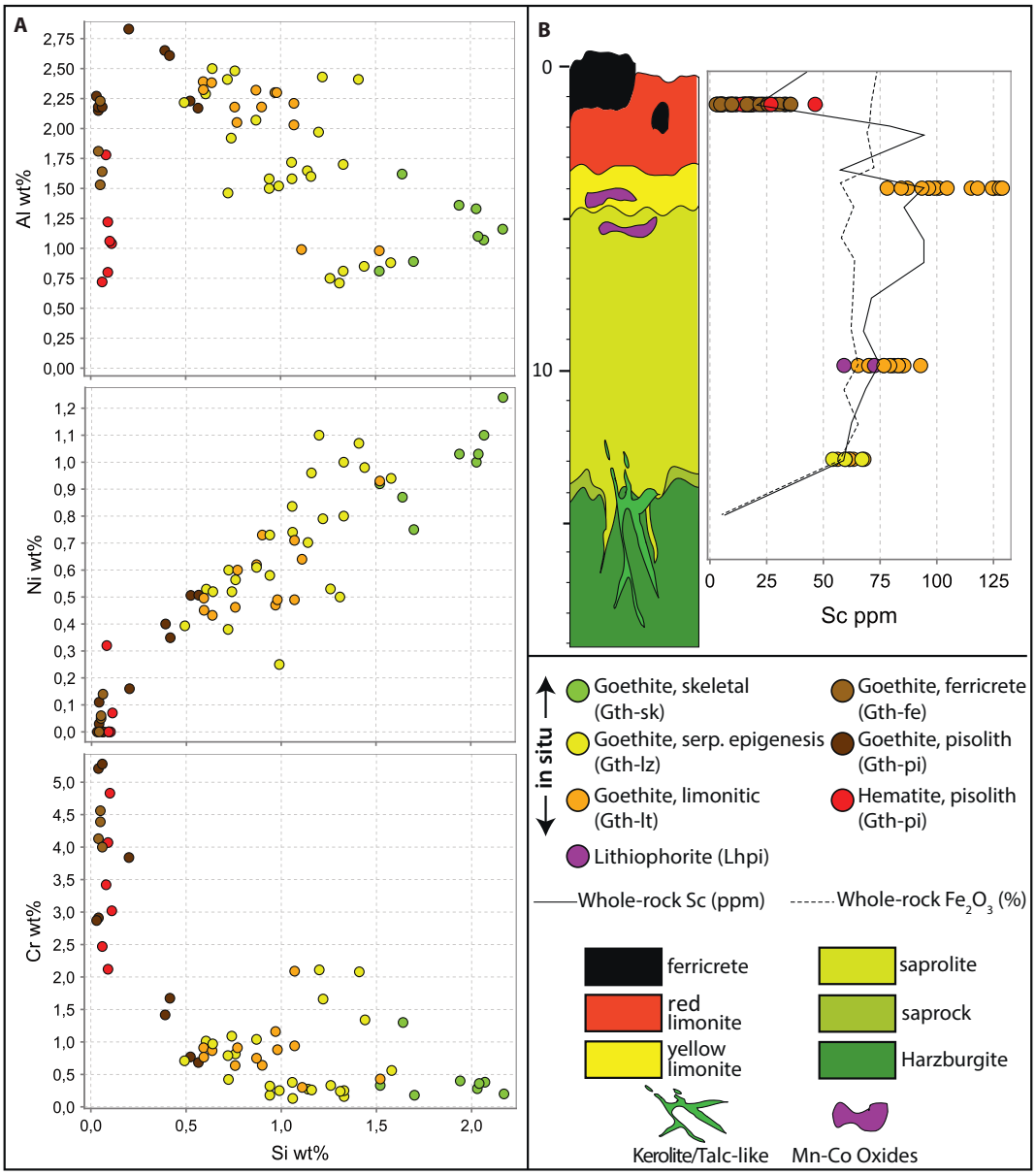

Fig. 17. (A) Plots of Al, Cr and Ni as a function of Si (wt%) in goethite and hematite from the harzburgite-derived OPB7 profile, Koniambo (WDS data). (B) Evolution of the Sc content of goethite in the OPB7 profile (LA-ICP-MS data) and comparison with whole-rock Sc and Fe_2O_3 concentration patterns.

observed decrease in Sc concentrations from the yellow to the red limonite. The observation that Sc accumulates in goethite-rich saprolitized amphibolites whereas it is largely transferred from hematite-rich lateritized gabbros to the surrounding goethite-rich limonite, also relates to the higher affinity of Sc with goethite than with hematite. The striking discrepancy in the nature of secondary iron carriers between peridotite- and amphibolite-derived alterites on one hand (mostly goethite) and gabbro-derived alterites (mostly hematite) on the other is facies-dependant and commonly observed down to the outcrop scale (e.g in the South Alpha pit, Tiébaghi, Fig. 4B). Such discrepancy likely results either from differences in the activity of water, pH and/or Al/Fe ratio (Schwertmann et al., 2000; Trolard and Tardy, 1989; Ramanaidou, 1989). With regards to the activity of water, high drainage conditions in lateritic profiles favor the maintenance of unsaturated zones at great depths wherein hematite predominates over goethite (Trolard and Tardy, 1989). Conversely, poor drainage conditions lead to water saturation at shallower depths and favor goethite over hematite. With regards to pH, goethite formation is optimal both at low (pH = 4) and high (pH = 12) pH, whereas hematite formation is optimal at near neutral (pH = 8) pH ratio (Cornell and Schwertmann, 1996; Schwertmann and Murad, 1983; Schwertmann et al., 2000). Eventually, increase in the Al/Fe ratio favors hematite over goethite (Schwertmann and Stanjek, 1998; Schwertmann et al., 2000). We proposed that the high Al/Fe ratio in gabbro favors the formation of hematite during weathering. Conversely, the low to moderate Al/Fe ratio in peridotite and pyroxenite/amphibolite favors the formation of goethite. It is noteworthy that changes in water activity may also be involved in the observed mineral discrepancy. Subvertical, readily altered gabbros likely constitute preferential drain pathways for weathering fluids, allowing the maintenance of unsaturated conditions at much greater depths compared to surrounding lateritized peridotites. In contrary, amphibolites and pyroxenites are more resistant to alteration and probably act as aquitards for both lateral and downwards fluid circulation.

Therefore, it is proposed that three main factors control the distribution and intensity of Sc enrichment in peridotite-, amphibolite- and gabbro-derived laterites. The first critical factor for the formation of Sc-rich zones in laterites is the occurrence of parent rocks that have a

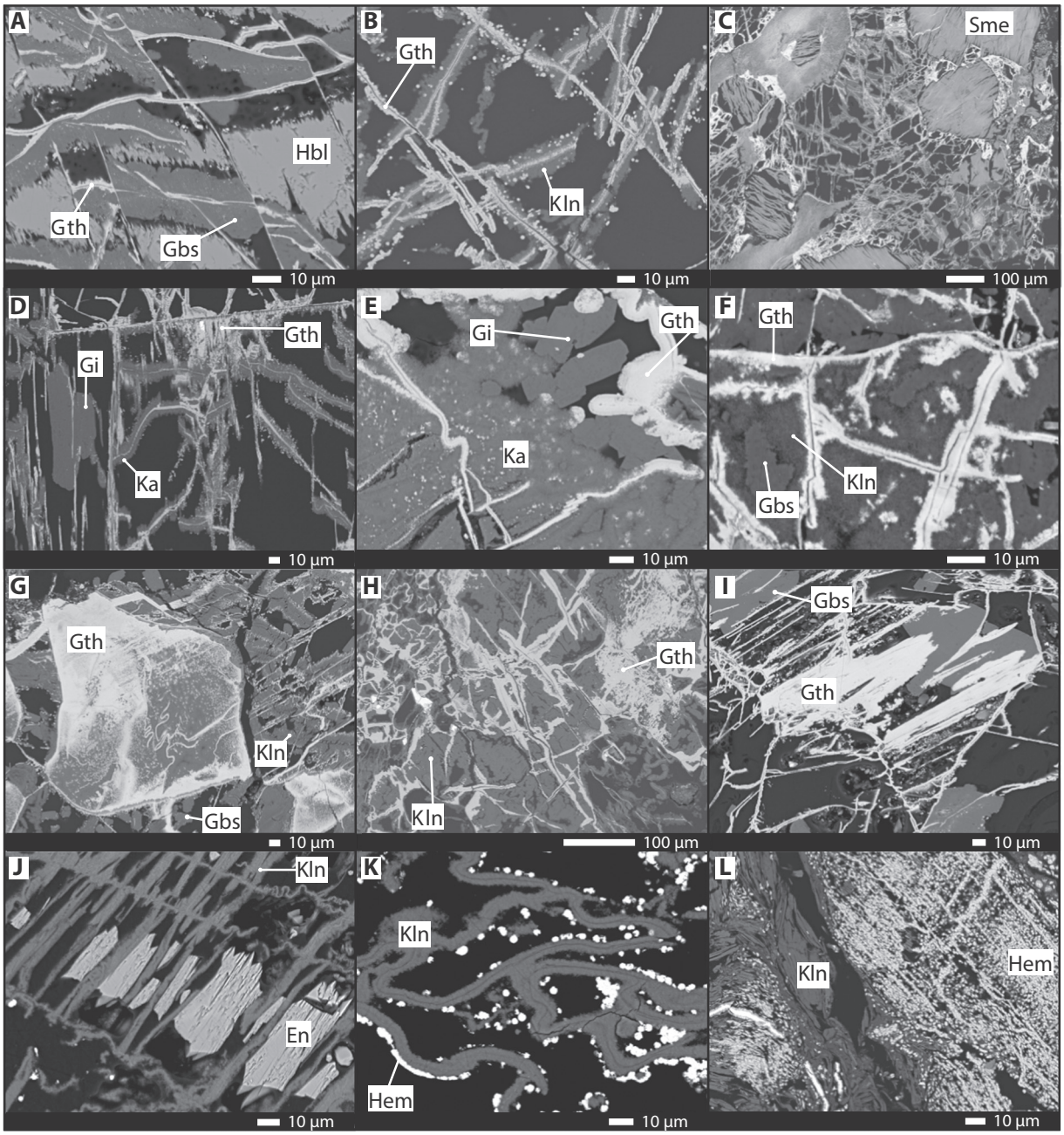

Fig. 18. Backscattered Electron (BSE) microphotographs: (A–I) amphibolite-derived saprolite. (J–L) gabbro-derived saprolite and laterite. Hbl = hornblende, Gth = goethite, Gbs = gibbsite, Kln = kaolinite, En = enstatite, Hem = hematite.

strong potential (fertility) for subsequent upgrade and mineralization. Unweathered mafic and ultramafic rocks exhibit a large range of Sc concentrations from < 5 ppm in dunite to > 10 ppm in lherzolite and up to 100 ppm or higher in amphibolite. Such variations are primarily controlled by the relative proportion of Sc-bearing primary phases, mostly enstatite and hornblende in peridotites and intrusive rocks, respectively. In peridotites, significant variations in the Sc content of enstatite are also observed depending on the considered peridotitic massif, with higher concentrations observed within lherzolites of the Tiébaghi massif. In intrusive rocks, Sc-bearing hornblende exhibit very large variations of the Sc content down to the outcrop scale. The crystal chemistry of Sc in primary silicates remains to be further investigated. It is however suggested that Sc^{3+} in silicates occurs in 6-fold coordination (Horovitz, 2012) and may replace Fe^{2+} and Mg^{2+}, as these have similar ionic radii. The second critical element for the formation of Sc-rich laterites is the maintenance of long-lived tropical weathering allowing acidic, Si-under saturated meteoric fluids to dissolve primary minerals and leach away most cations including Si. This favors the concentration of iron as goethite together with other poorly mobile elements including Sc. Third, further maturation of peridotite- and amphibolite-derived lateritic profiles favors both the dissolution/recrystallization of goethite and its replacement by hematite, both processes likely resulting in the local remobilization and concentration of Sc in the directly underlying horizons. In a similar manner, the preferential hematitization of gabbros during weathering results in the transfer and concentration of Sc in surrounding goethite-rich zones. In any case, the formation of goethite is of critical importance as it is the predominant mineral trap for Sc. The chemical speciation of Sc in goethite remains to be investigated as it probably has important implications both for further understanding of Sc mobility in laterites as well as for the fine-

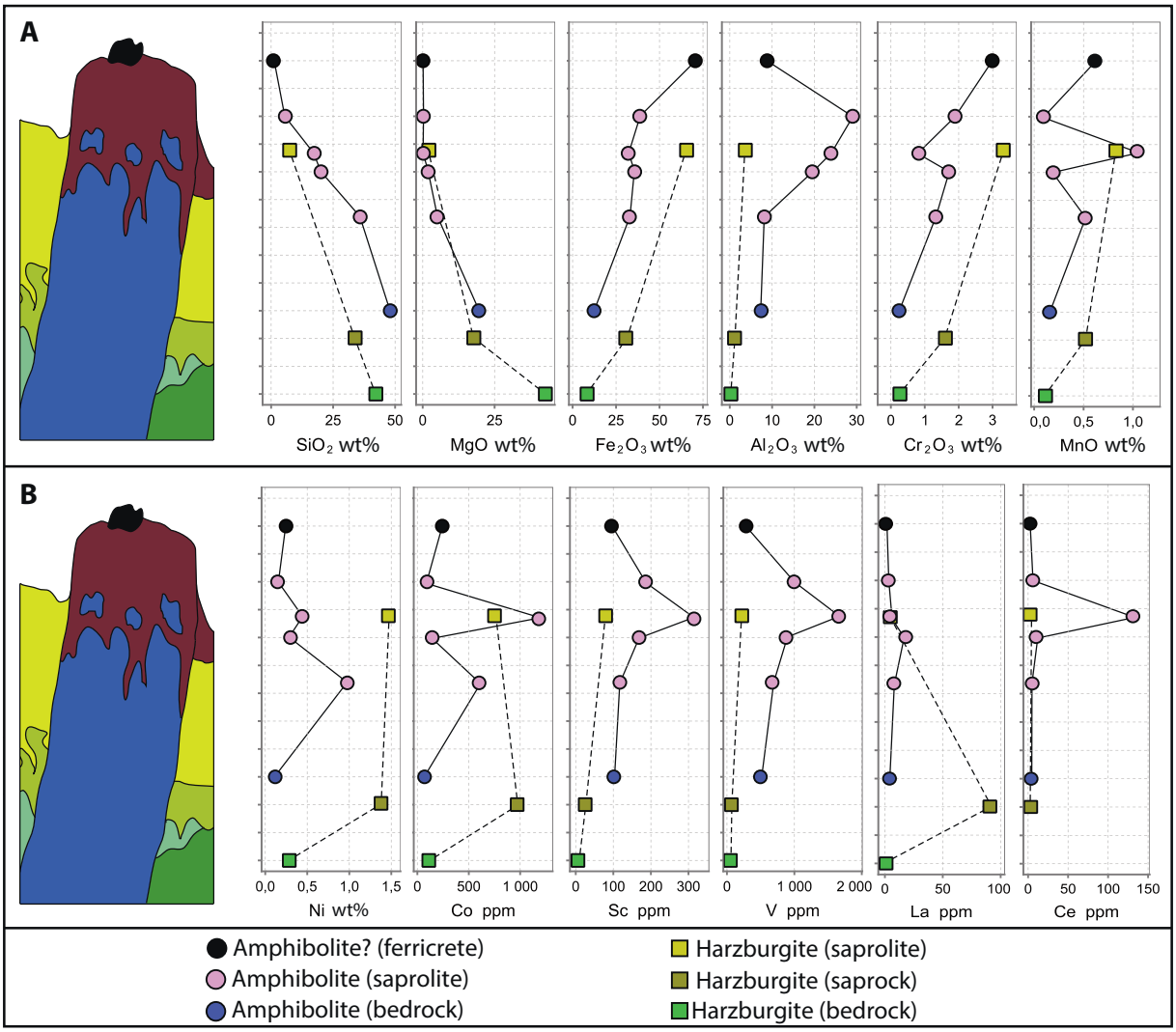

Fig. 19. Geochemical evolution along amphibolite-derived laterite profile NGPB (N'Go): (A) Major oxides: SiO_2, MgO, Fe_2O_3, Al_2O_3, Cr_2O_3, MnO (wt%), (B) Economic elements: Ni (wt%), Co (ppm), Sc (ppm), trace and LREE: V, La, Ce (ppm).

tuning of metallurgical Sc extraction processes.

7.2. Implications for Sc exploration and mining in New Caledonia

A possible exploration strategy for identifying peridotite-derived Ni laterites wherein the Sc content is high enough to make it a potentially attractive by-product of Ni (and Co) production includes:

- The recognition of fertile peridotitic parent rocks. Harzburgite and lherzolite are the most fertile types of peridotite as they contain significant proportions of Sc-bearing enstatite (and more marginally diopside). This study has demonstrated that Al and V are reliable pathfinder elements indicative of the Sc content in unweathered peridotites regardless their degree of serpentinization. At the deposit scale, the analysis of the Al (and V) content of unweathered peridotites may therefore complement field-based recognition of peridotite facies, especially in strongly serpentinized zones.
- The recognition of Sc-rich limonitic horizons and their degree of overlap with Ni(-Co)-rich zones. As Sc is most enriched in the yellow limonite horizons, zones of maximum Sc enrichment do not coincide with zones of maximum Ni (and Co) enrichment. Yet, determination of respective Ni, Co and Sc cut-off grades based on stock prices and production costs considerations may allow identification of overlapping zones wherein covalorization of lateritic Ni, Co and Sc may be economically viable while Ni grades remain too low to be attractive for a standalone commodity production. There, as for unweathered peridotites, the analysis of the Al and V concentrations may be indicative of Sc grades. Also, the occurrence of hematite-bearing, gabbro-derived laterites cutting across peridotite-derived, yellow limonitic horizons is likely associated with Sc enrichment localized within a few meters from the gabbro salbands. Field-based recognition of gabbro-derived laterites is relatively straightforward and may be taken into consideration for target ranking prior to drill testing.

In addition to the potential covalorization of Ni, Co and Sc in peridotite-derived laterites, saprolitized amphibolites may represent attractive targets for primary Sc production. However, this study has shown that amphibolites exhibit large variations in their Sc content, both in unweathered facies and in their weathered derivatives, and that they represent discrete occurrences of relatively restricted volumes. Following the field-based recognition of amphibolite-bearing intrusions, the identification of fertile amphibolites may be based on textural observation to determine the relative proportion and crystal size of hornblende, with preference for pegmatoïd textures. Also, analysis of Ti and V in amphibolites may provide first order estimates of their Sc content.

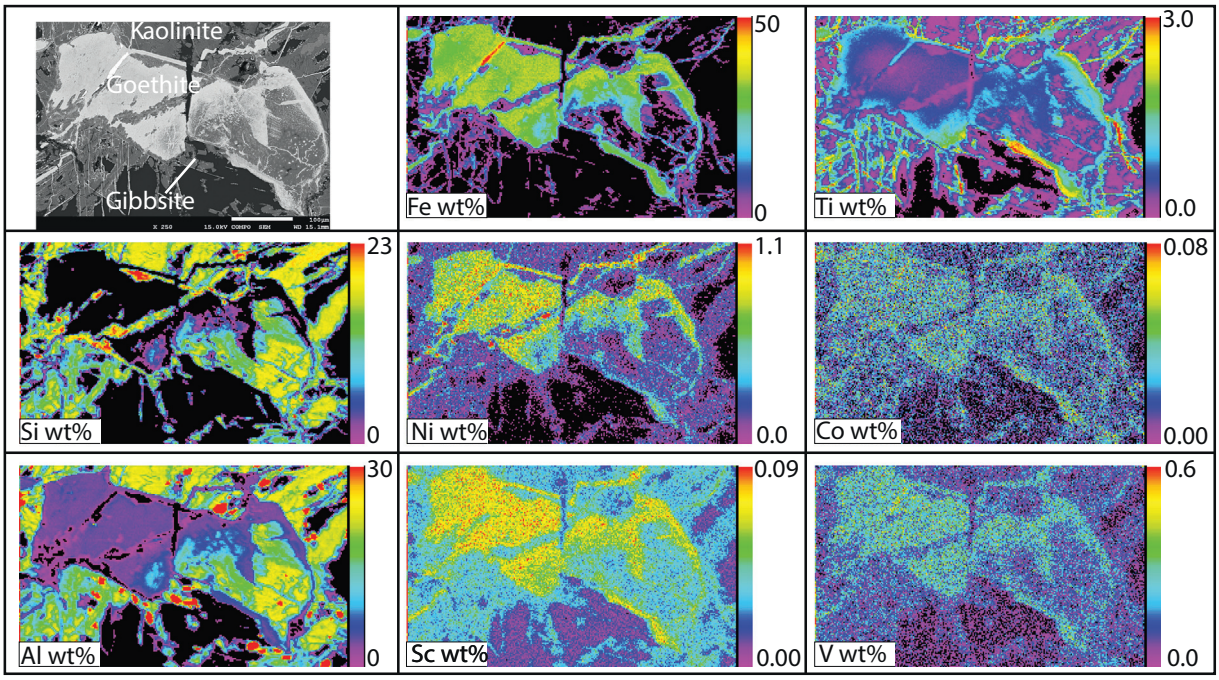

Fig. 20. Quantitative elementary maps (Fe, Ti, Si, Ni, Co, Al, Sc, V; wt%) of a goethite – kaolinite – gibbsite mineral assemblage developed in amphibolite-derived saprolite (NGPB profile, N'Go).

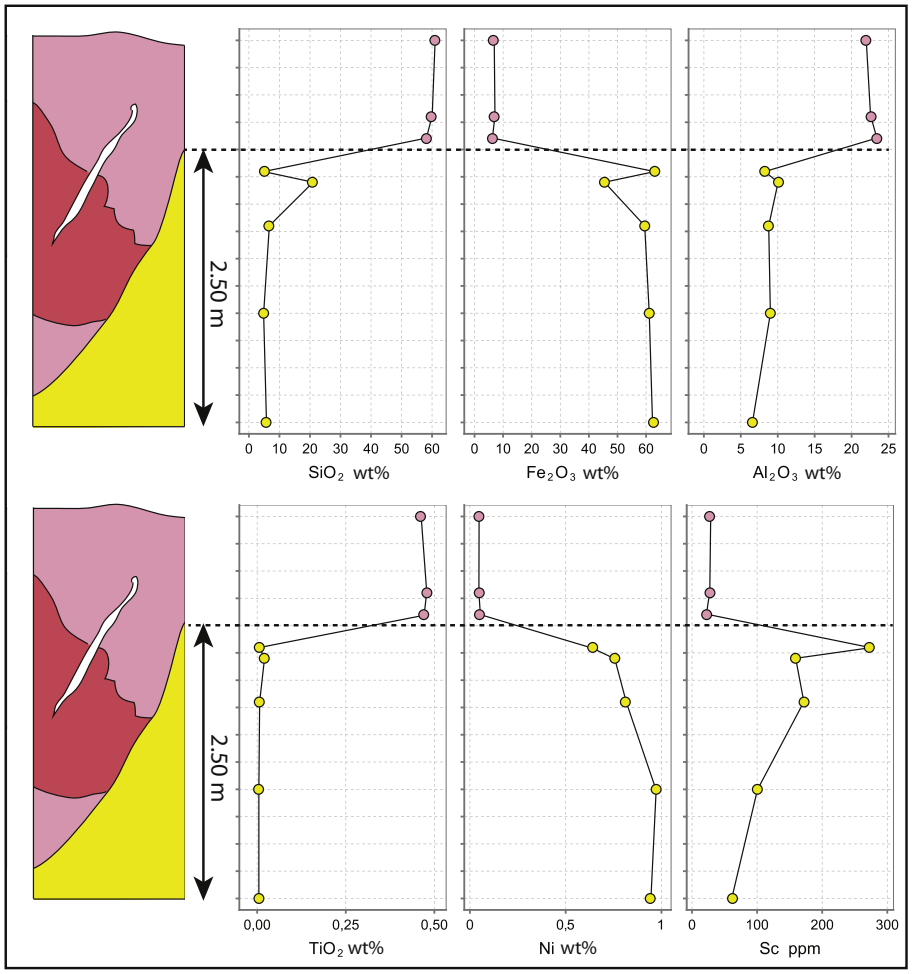

Fig. 21. Geochemical trends in gabbro-derived lateritic profile KNGA (Koniambo): Major oxides: SiO_2, Fe_2O_3, Al_2O_3, TiO_2 (wt%), economic elements: Ni (wt%), Sc (ppm).

8. Conclusion

This contribution examines the distribution and the critical controls on the formation of Sc-rich zones within New Caledonian laterites. The yellow limonitic zones of some peridotite-derived Ni laterites exhibit elevated Sc concentrations up to 100 ppm, suggesting the potential for co-valorization along with Ni and Co production. Spatially restricted, amphibolite-derived saprolites are also host to remarkable Sc concentrations up to > 300 ppm.

The initial Sc content of unweathered parent rocks represent the first critical control on the maximum Sc grades reached in their lateritized derivatives. In unweathered peridotites, enstatite is the dominant Sc host, controlling the Sc content of harzburgite and lherzolite. In intrusive mafic to ultramafic rocks, hornblende is the dominant Sc host, controlling the Sc content of hornblende-bearing intrusive rocks. In all investigated lateritic profiles, residual Sc enrichment in the upper, goethite-dominated horizons constitutes the second critical condition for the development of Sc-rich zones. Third, the expulsion of Sc from the uppermost horizons and downwards concentration following goethite recrystallization and/or hematitization leads to further Sc enrichment. In peridotite-derived Ni laterites, the increase in the Sc content corresponds to a ~tenfold enrichment compared to the parent peridotite. The occurrence of elevated Sc concentrations up to 100 ppm in the yellow limonitic zones of harzburgite- and lherzolite-derived Ni laterites suggests the potential for co-valorization along with Ni and Co production, providing that Sc-rich zones sufficiently overlap low-grade lateritic Ni(-Co) ore zones. In amphibolite-derived saprolites, Sc-bearing goethite yields Sc concentrations up to 800 ppm but occurs in association with gibbsite and/or kaolinite so that maximum bulk rock Sc concentrations only grades up to ~300 ppm, corresponding to a two- to threefold increase of the Sc content compared to the parent rock. Such concentrations may be economically attractive for standalone Sc production, although high-grade saprolitized amphibolites represent marginal volumes especially when compared to high-grade Sc deposits recognized in Australia (Chassé et al., 2017). Contrasting with peridotites and amphibolites, the lateritization of gabbros leads to the preferential formation of hematite rather than goethite, resulting in significant remobilization of Sc and subsequent trapping in the surrounding goethite-rich, peridotite-derived Ni laterite. There, enrichment up to > 150–200 ppm may add significant value to the prospective co-recovery of Ni-Co-Sc.

Acknowledgments

This work has been funded and logistically supported by the French National Research Agency through the national program "Investissements d'avenir" of the Labex Ressources 21 with the reference ANR-10-LABX-21-RESSOURCES21 and by the National Centre for Technological Research CNRT "Nickel et son environnement" based in Nouméa, New Caledonia (Project grant: 8PS2013-CNRT.CNRS/SCANDIUM). The authors would like to thank, Stephane Lesimple and Dr. Bernard Robineau from the Geological Survey of New Caledonia, together with France Bailly and Laurence Barriller from the National Centre for Technological Research, for their technical and logistical support as well as for sharing their extensive knowledge of the geology of New Caledonia. We are grateful to Société Le Nickel (SLN), Koniambo Nickel SAS (KNS), Nickel Mining Company (NMC), Société des Mines de la Tontouta (SMT) and Mai Kouaoua Mines (MKM) for support and access to mines and drill cores. In particular, we acknowledge Dr. Mohamed Kadar (SLN), Dr. Clément Marcaillou (SLN), Dr. Maxime Drouillet (KNS), Willy Foucher (NMC), Mathieu Mazières (SMT), Matthieu Muret (SMT) and Matthieu Désesquelles (MKM) for their involvement. We also thank Dr. Christophe Cloquet (SARM analytical centre, CRPG, Vandœuvre-lès-Nancy, France), Dr. Marie-Christine Boiron, Dr. Chantal Peiffert, Dr. Andreï Lecomte and Dr. Olivier Rouer (GeoRessources, Vandœuvre-lès-Nancy, France) for technical support in providing analytical data.

Declarations of interest

None.

Appendix A. Supplementary data

Supplementary data to this article can be found online at https://doi.org/10.1016/j.gexplo.2018.10.009.

References

Aiglsperger, T., Proenza, J.A., Lewis, J.F., Labrador, M., Svojtka, Rojas-Puron, A., Longo, F., Durisova, J., 2016. Critical metals (REE, Sc, PGE) in Ni laterites from Cuba and the Dominican Republic. Ore Geol. Rev. 76 (1), 127–147.

Altinsel, Y., Topkaya, Y., Topkaya, Kaya, S., Şentürk, B., 2018. Extraction of scandium from lateritic nickel-cobalt ore leach solution by ion exchange: a special study and literature review on previous works. In: Martin, O. (Ed.), Light Metals 2018. TMS 2018. The Minerals, Metals & Materials Series. Springer, Cham.

Ambrosi, J.P., Nahon, D., Herbillon, A.J., 1986. The epigenetic replacement of kaolinite by hematite in laterite - petrographic evidence and the mechanisms involved. Geoderma 37, 283–294.

Audet, M., 2008. Le massif du Koniambo, Nouvelle-Calédonie. Formation et obduction d'un complexe ophiolitique du type SSZ. Enrichissement en nickel, cobalt et scandium dans les profils résiduels. Ph.D thesis. Université de la Nouvelle Calédonie/Université du Quebec à Montréal (326 pp).

Avias, J., 1967. Overthrust structure of the main ultrabasic New Caledonian massives. Tectonophysics 4, 531–541.

Bailly, L., Ambrosi, J.P., Barbarand, J., Beauvais, A., Cluzel, D., Lerouge, C., Prognon, C., Quesnel, F., Ramanaïdou, E., Ricordel-Prognon, C., Ruffet, G., Sevin, B., Wells, L., Yans, J., 2014. Projet NICKAL: "Typologie des minerais latéritiques de Nouvelle-Calédonie et facteurs de concentration de Co et Ni", rapport final, BRGM/RP-63 482-FR. (402 pp).

Butt, C.R.M., Cluzel, D., 2013. Nickel laterite ore deposits: weathered serpentinites. Elements 9, 123–128.

Carignan, J., Hild, P., Mevelle, G., Morel, J., Yeghicheyan, D., 2001. Routine analyses of trace elements in geological samples using flow injection and low pressure on-line liquid chromatography coupled to ICP-MS: a study of geochemical reference materials BR, DR-N, UB-N, AN-G and GH. Geostand. Geoanal. Res. 25 (2–3), 187–198.

Cathelineau, M., Quesnel, B., Gautier, P., Boulvais, P., Couteau, C., Drouillet, M., 2016. Nickel dispersion and enrichment at the bottom of the regolith: formation of pimelite target-like ores in rock block joints (Koniambo Ni deposit, New Caledonia). Mineral. Deposita 51 (2), 271–282.

Cathelineau, M., Myagkiy, A., Quesnel, B., Boiron, M.-C., Gautier, P., Boulvais, P., Ulrich, M., Truche, L., Golfier, F., Drouillet, M., 2017. Multistage crack seal vein and hydrothermal Ni enrichment in serpentinized ultramafic rocks (Koniambo massif, New Caledonia). Mineral. Deposita 52 (7), 945–960.

Chardon, D., Chevillotte, V., 2006. Morphotectonic evolution of the New Caledonia ridge (Pacific Southwest) from post-obduction tectonosedimentary record. Tectonophysics 420, 473–491.

Chassé, M., Griffin, W.L., O'Reilly, S.Y., Calas, G., 2017. Scandium speciation in a world-class lateritic deposit. Geochem. Perspect. Lett. 3, 105–114.

Cluzel, D., Aitchison, J.C., Picard, C., 2001. Tectonic accretion and underplating of mafic terranes in the Late Eocene intraoceanic fore-arc of New Caledonia (Southwest Pacific): geodynamic implications. Tectonophysics 340 (1–2), 23–59.

Cluzel, D., Meffre, S., Maurizot, P., Crawford, A.J., 2006. Earliest Eocene (53 Ma) convergence in the Southwest Pacific: evidence from pre-obduction dikes in the ophiolite of New Caledonia. Terra Nova 18, 395–402.

Cluzel, D., Maurizot, P., Collot, J., Sevin, B., 2012a. An outline of the Geology of New Caledonia; from Permian–Mesozoic Southeast Gondwanaland active margin to Cenozoic obduction and supergene evolution. Episodes 35 (1), 72–86.

Cluzel, D., Jourdan, F., Meffre, S., Maurizot, P., Lesimple, S., 2012b. The metamorphic sole of New Caledonia ophiolite: 40Ar/39Ar, U-Pb, and geochemical evidence for subduction inception at a spreading ridge. Tectonics 31, 1–18.

Cornell, R.M., Schwertmann, U., 1996. The Iron Oxides. Structure, Properties, Reactions, Occurrence and Uses. VCH Verslagsgesellschaft, Weinheim.

Das, H.A., Zonderhuis, J., van der Marel, H.W., 1971. Scandium in rocks, minerals and sediments and its relations to iron and aluminium. Contrib. Mineral. Petrol. 32 (3), 231–244.

Dublet, G., Julliot, F., Morin, G., Fritsch, E., Fandeur, D., Brown Jr., G.E., 2015. Geochim. Cosmochim. Acta 160, 1–15.

Emsley, J., 2014. Unsporting scandium. Nat. Chem. 6, 1025.

Ferizoglu, E., Kaya, S., Topkaya, Y.A., 2018. Solvent extraction behaviour of scandium from lateritic nickel-cobalt ores using different organic reagents. Physicochem. Probl. Miner. Process. 54 (2), 538–545.

Freyssinet, P.H., Butt, C.R.M., Morris, R.C., Piantone, P., 2005. Ore-forming processes related to lateritic weathering. In: Hedenquist, J.W., Thomson, J.F.H., Goldfarb, R.J., Richards, J.P. (Eds.), Economic Geology 100th Anniversary Volume. Economic Geology Publishing Company, New Haven, Connecticut, pp. 681–722.

Frost, B.R., Evans, K.A., Swapp, S.M., Beard, J.S., Mothersole, F.E., 2013. The process of serpentinization in dunite from New Caledonia. Lithos 178, 24–39.

Genna, A., Maurizot, P., Lafoy, Y., Augé, T., 2005. Role of karst in the nickeliferous mineralisations of New Caledonia. Compt. Rendus Geosci. 337 (3), 367–374.
Golightly, J.P., 2010. Progress in understanding the evolution of nickel laterites. In: Goldfarb, R.J., Marsh, E.E., Monecke, T. (Eds.), The Challenge of Finding New Mineral Resources: Global Metallogeny, Innovative Exploration, and New Discoveries Volume II. 15. Society of Economic Geologists Special Publication, pp. 451–475.
Guillon, J.H., 1975. Les massifs péridotitiques de Nouvelle-Calédonie. Mémoires 76 (120 pp., ORSTOM, Paris).
Guillong, M.M., Maier, D.L., Allan, M.M., Heinrich, C.A., 2008. SILLS: a MATLAB based program for the reduction of laser ablation ICPMS data of homogeneous materials and inclusions. In: Sylvester, P. (Ed.), Laser Ablation ICPMS in the Earth Sciences. Current Practices and Outstanding Issues, pp. 328–333.
Hoatson, D.M., Jaireth, S., Miezitis, Y., 2011. The major rare-earth-element deposits of Australia: geological setting, exploration, and resources. Geosci. Australia 58–63. https://d28rz98at9flks.cloudfront.net/71820/Complete_Report.pdf.
Horovitz, C.T., 2012. Biochemistry of Scandium and Yttrium, Part 1: Physical and Chemical Fundamentals. Springer Science & Business Media, New York (324 pp).
Jeanpert, J., Genthon, P., Maurizot, M., Folio, J.L., Vendé-Leclerc, M., Sérino, J., Join, J.L., Iseppi, M., 2016. Morphology and Distribution of Dolines on Ultramafic Rocks From Airborne LiDAR Data: The Case of Southern Grande Terre in New Caledonia (SW Pacific).
Latham, M., 1986. Altération et pédogenèse sur roches ultrabasique en Nouvelle Caledonie. Genèse et évolution des accumulations de fer et de silice en relation avec la formation du modéle. ORSTOM, Dijon (Thèse d'état, 331 pp.).
Manceau, A., Schlegel, M.L., Musso, M., Sole, V.A., Gauthier, C., Petit, P.E., Trolard, F., 2000. Crystal chemistry of trace elements in natural and synthetic goethite. Geochim. Cosmochim. Acta 64 (21), 3643–3661.
Marchesi, C., Garrido, C.J., Godard, M., Belleyd, F., Ferré, E., 2009. Migration and accumulation of ultra-depleted subduction-related melts in the Massif du Sud ophiolite (New Caledonia). Cemical Geol. 266 (3–4), 171–186.
Maulana, A., Sanematmatmatsu, K., Sakakibara, M., 2016. An Overview on the Possibility of Scandium and REE Occurrence in Sulawesi, Indonesia. Indones. J. Geosci. 3, 139–147.
Maurizot, P., Vendé-Leclerc, M., 2009. New Caledonia Geological Map, Scale 1/500 000. Direction de l'Industrie, des Mines et de l'Énergie – Service de la Géologie de Nouvelle-Calédonie, Bureau de Recherches Géologiques et Minières.
Mortimer, N., Campbell, H.J., Tulloch, A.J., King, P.R., Stagpoole, V.M., Wood, R.A., Rattenbury, M.S., Sutherland, R., Adams, C.J., Collot, J., Seton, M., 2017. Zealandia: Earth's hidden continent. GSA Today 27 (3), 27–35.
Orberger, B., Lorand, J.P., Girardeau, J., Mercier, J.C.C., Pitragool, S., 1995. Petrogenesis of ultramafic rocks and associated chromitites in the Nan Uttaradit ophiolite, Northern Thailand. Lithos 35, 153–182.
Orloff, O., 1968. Etude géologique et géomorphologique des massifs d'ultrabasites compris entre Houailou et Canala (Nouvelle-Calédonie). Univ. Montpellier, France (PhD thesis, 189 pp).
Paquette, J.L., Cluzel, D., 2007. U–Pb zircon dating of post-obduction volcanic-arc granitoids and a granulite-facies xenolith from New Caledonia. Inference on Southwest Pacific geodynamic models. Int. J. Earth Sci. 96 (4), 613–622.
Prinzhofer, A., 1981. Structure et pétrologie d'un cortège ophiolitique: le Massif du Sud (Nouvelle-Calédonie). La transition manteau-croûte en milieu océanique. Ecole Normale Supérieure des Mines, Paris, France (PhD thesis, 185pp).
Quesnel, B., Gautier, P., Boulvais, P., Cathelineau, M., Maurizot, P., Cluzel, D., Ulrich, M., Guillot, S., Lesimple, S., Couteau, C., 2013. Syn-tectonic, meteoric water-derived carbonation of the New Caledonia peridotite nappe. Geology 41, 1063–1066.
Ramanaidou, E.R., 1989. Genèse d'un gisement latéritique, Evolution supergène des itabirites Protérozoiques de la mine de fer de Capanema (Minas Gerais, Brésil). University of Poitiers (PhD thesis, 183 pp).
Ricketts, N.J., Duyvesteyn, W.P.C., 2018. Scandium recovery from the Nyngan Laterite Project in NSW. In: Martin, O. (Ed.), Light Metals 2018. TMS 2018. The Minerals, Metals & Materials Series. Springer, Cham.
Royset, J., Ryum, N., 2005. Scandium in aluminium alloys. Int. Mater. Rev. 50 (1), 19–44.
Rudnick, R.L., Gao, S., Holland, H., Turekian, K.K., 2014. Composition of the continental crust. In: Treatise on Geochemistry, 2nd edition. Elsevier Ltd, Amsterdam, Netherlands, pp. 1–51.
Schwertmann, U., Latham, M., 1986. Properties of iron oxides in some New Caledonian oxisols. Geoderma 39, 105–123.
Schwertmann, U., Murad, E., 1983. Effect of pH on the formation of goethite and hematite from ferrihydrite. Clay Clay Miner. 31 (4), 277–284.
Schwertmann, U., Stanjek, H., 1998. Stirring effects on properties of Al goethite formed from ferrihydrite. Clay Clay Miner. 46 (3), 317–321.
Schwertmann, U., Friedl, J., Stanjek, H., Schulze, D.G., 2000. The effect of Al on Fe oxides. XIX. Formation of Al-substituted hematite from ferrihydrite at 25 °C and pH 4 to 7. Clay Clay Miner. 48 (2), 159–172.
Sevin, B., Ricordel-Prognon, C., Quesnel, F., Cluzel, D., Lesimple, S., Maurizot, P., 2012. First palaeomagnetic dating of ferricrete in New Caledonia: new insight on the morphogenesis and palaeoweathering of 'Grande Terre'. Terra Nova 24, 77–85.
Sevin, B., Cluzel, D., Maurizot, P., Ricordel-Prognon, C., Chaproniere, G., Folcher, N., Quesnel, F., 2014. A drastic lower Miocene regolith evolution triggered by post obduction slab break-off and uplift in New Caledonia. Tectonics 33 (9), 1787–1801.
Toropova, L.S., Eskin, D.G., Kharakterova, M.L., Dobatkina, T.V., 1998. Advanced Aluminium Alloys Containing Scandium. Structure and Properties, Gordon and Breach. Science Publishers, Amsterdam, pp. 175.
Trescases, J.-J., 1975. L'evolution Géochimique Supergène des Roches Ultrabasiques en Zone Tropicale: Formation des Gisements Nickélifères de Nouvelle-Calédonie Edited. O.R.S.T.O.M., France, Paris.
Trolard, F., Tardy, Y., 1989. A model of Fe^{3+}-kaolinite-Al^{3+}-goethite-Al^{3+}-hematite equilibria in laterites. Clay Miner. 24, 1–21.
Trolard, F., Bourrie, G., Jeanroy, E., Herbillon, A.J., Martin, H., 1995. Trace metals in natural iron oxides from laterites: a study using selective kinetic extraction. Geochim. Cosmochim. Acta 59 (7), 1285–1297.
U.S. Geological Survey, 2018. Scandium. In: Mineral Commodity Summaries. U.S. Geological Survey, Reston, USA, pp. 144–145.
Ulrich, M., 2010. Péridotites et serpentinites du complexe ophiolitique de la Nouvelle-Calédonie. Université Joseph Fournier – Université de la Nouvelle-Calédonie (PhD thesis, 272 pp).
Ulrich, M., Picard, C., Guillot, S., Chauvel, C., Cluzel, D., Meffre, S., 2010. Multiple melting stages and refertilization as indicators for ridge to subduction formation: the New Caledonia ophiolite. Lithos 115, 223–236.
Ulrich, M., Muñoz, M., Boulvais, P., Cathelineau, M., Guillot, S., Picard, C., Putlitz, B., 2016. Geochemistry of the New Caledonia serpentinites: evidences for multiple serpentinization events at various depths. In: Serpentine Days. 2016.
Ulrich, M., Cathelineau, M., Boiron, M.-C., Muñoz, M., Teitler, Y., Karpoff, A.-M., 2018. Critical (Sc, REE) and transitional metal enrichments in Ni laterite deposits of New Caledonia. J. Geochem. Explor (submitted).
Wang, W., Pranolo, Y., Cheng, C.Y., 2011. Metallurgical processes for scandium recovery from various resources: a review. Hydrometallurgy 108 (1–2), 100–108.
Wells, M.A., Ramanaidou, E.R., Verrall, M., Tessarolo, C., 2009. Mineralogy and crystal chemistry of "garnierites" in the Goro lateritic nickel deposit, New Caledonia. Eur. J. Mineral. 21 (2), 467–483.